Identification of Novel Potent and Non-toxic Anticancer, Anti-Angiogenic and Antimetastatic Rhenium Complexes against Colorectal Carcinoma

Joachim Delasoie [1], Aleksandar Pavic [2,*], Noémie Voutier [1], Sandra Vojnovic [2], Aurelien Crochet [1], Jasmina Nikodinovic-Runic [2,*] and Fabio Zobi [1,*]

[1] Department of Chemistry, Fribourg University, Chemin du Musée 9, 1700 Fribourg, Switzerland

[2] Institute of Molecular Genetics and Genetic Engineering, University of Belgrade, Vojvode Stepe 444a, 11042 152 Belgrade, Republic of Serbia

* Correspondence: fabio.zobi@unifr.ch (F.Z.), sasapavic@imgge.bg.ac.rs (A.P.), jasmina.nikodinovic@imgge.bg.ac.rs (J.N.R.)

Abstract: Combination therapy targeting both tumor growth and vascularization is considered to be a cornerstone for colorectal carcinomas (CRC) treatment. However, the major obstacles of most clinical anticancer drugs are their weak selective activity towards cancer cells and inherent inner organs toxicity, accompanied with fast drug resistance development. In our effort to discover novel selective and non-toxic agents effective against CRC, we designed, synthesized and characterized a series of rhenium(I) tricarbonyl-based complexes with increased lipophilicity. Two of these novel compounds were discovered to possess remarkable anticancer, anti-angiogenic and antimetastatic activity *in vivo* (zebrafish-human HCT-116 xenograft model), being effective at very low doses (1-3 μM). At doses as high as 250 μM the complexes did not provoke toxicity issues encountered in clinical anticancer drugs (cardio-, hepato-, and myelotoxicity). *In vivo* assays showed that the two compounds exceed the anti-tumor and anti-angiogenic activity of clinical drugs cisplatin and sunitinib malate, and display a large therapeutic window.

Keywords: colorectal carcinoma; rhenium; zebrafish; xenograft; angiogenesis; antimetastatic.

Highlights

- Re(I) tricarbonyl complexes **1** and **4** had selective cytotoxicity towards HCT-116 cells
- **1** and **4** had potent antitumor and antimetastatic activity in HCT-116 xenograft model
- **1** and **4** have comparable or higher anti-angiogenic potential than sunitinib-malate
- **1** and **4** are not toxic at very high dose and have large therapeutic window
- Complexes **1** and **4** are accumulated within the lysosomes and the cytoplasm

Introduction

The latest report released by the International Agency for Research on Cancer indicated that cancer burden worldwide has risen to 18.1 million new cases and 9.6 million cancer deaths in 2018, while the statistical forecasts provided by WHO estimate more than 21 million new cancer cases and 13 million deaths by 2030 [1]. Among all cancer types, colorectal carcinomas (CRC) are amongst the most aggressive cancers globally, being ranked as third in terms of incidence and second in terms of mortality, and together with lung and breast cancers, are responsible for one third of the cancer incidence and mortality [1, 2]. This solid malignancy, characterized by high metastatic potential, accounts in Europe and Americas alone for more than 40% of the global cancer cases and deaths [1]. In current oncological practice, combination therapy based on the use of cytostatic and anti-angiogenic drugs is a cornerstone for CRC treatment since it simultaneously targets malignant cells and tumour vasculature [3]. However, a major problem responsible for the still high death incidence in CRC is the poor efficacy and low selectivity of clinically used anticancer drugs. Therefore, together with efficient prevention and early detection policies, new drugs and treatments are urgently required to complement and maintain existing therapies. With the aim of identify potentially new anticancer agents and to guide the formulation of new composite drug delivery systems, we have recently began a program centred on the use of frustules derived from unicellular microalgae for the targeted delivery of anticancer transition metal drugs to cancers, in particular, of the colorectum [4, 5].

Among inorganic and organometallic anticancer compounds, cisplatin and other platinum-based drugs have been used for decades in the treatment of a variety of neoplastic diseases. However, the clinical success of these drugs is limited by significant side effects, especially inherent nephrotoxicity and ototoxicity originating from the platinum element. Accordingly, the use of Re(I) tricarbonyl complexes is gaining momentum due to the advantageous characteristics of the species (high stability, low toxicity, structural diversity, rich spectroscopic properties, different mechanisms of action), making Re complexes potential anticancer therapeutics which may be suitable to enter clinical research and development. Compounds of the *fac*-$[Re(CO)_3]^+$ core (facial isomer of the rhenium tricarbonyl core) are robust, relatively straightforward to synthesize and can be properly designed to target specific cellular compartments. Due to their luminescent properties, these molecules can often be tracked intracellularly to correlate cellular and tissue distribution with their mode of action [6-10]. Furthermore, the reported antiproliferative activity of these

species on different cancer cell lines often equates or exceeds that of well-established inorganic drugs (e.g. cisplatin) [11].

The majority of anticancer *fac*-$[Re(CO)_3]^+$ compounds tested to date is that of *fac*-$[Re(CO)_3(\alpha\text{-diimine})L]^n$ type complexes where α-diimine are typically 2,2′-bipyridine or phenantroline-based ligands and L is a monodentate ligand (most often a pyridine derivative) or a halide (Cl, Br). However, examples of antiproliferative *fac*-$[Re(CO)_3]^+$ complexes of other bidentate ligand types, including N–O [12, 13], O-O [14] , P-P [15] and Se-Se chelates [16-20], N,N,N-tridentate chelates [21-26] or bridged di- or tri-nuclear alkoxo/hydroxo are also known [27-29]. Additionally, but rarer, phototoxic Re complexes capable of either generating reactive oxygen species (ROS) or liberating CO have also been identified [25, 30-33]. The former type of complexes act as photodynamic therapy photosensitizers, the latter, of general formula *fac*-$[Re(CO)_3(\alpha\text{-diimine})PR_3]^+$ (PR_3 = phosphine type-ligands) have been recently described by different authors [34-39]. Relatively recent and comprehensive reviews by Gasser *et al.* [11], Policar *et al.* [40], Lo *et al.* [41], Collery *et al.* [42], Kühn *et al.* [43] and Wilson *et al.* [44] have discussed the subject in detail, and it is apparent from these that the cytotoxicity of Re(I) tricarbonyl complexes is generally found to increase with lipophilicity [45-50] (most probably due to an improved cellular uptake) although exceptions do exist [51].

Within the context above, we therefore decided to explore the antiproliferative efficacy of a series of *fac*-$[Re(I)(CO)_3]^+$ N-derivatized N-([2,2'-bipyridin]-6-ylmethyl)-complexes of increasing lipophilicity against different cell lines, but with a focus on cells derived from CRC. In this study we report the synthesis, characterization and *in vitro* evaluation of this series of rhenium(I) tricarbonyl complexes as potential anticancer agents. In addition to that, we also report the detailed toxicity profile of the molecules in the zebrafish model as well as the anticancer/antimetastatic efficacy and effective inhibition of angiogenesis in the zebrafish xenograft model of human CRC. We found that at least two new molecules possess remarkable anticancer, anti-angiogenic and antimetastatic activity being effective at very low doses (1-3 μM) *in vivo*, and exceeding the potency of clinical drugs cisplatin and sunitinib malate. The most potent compounds (*vide infra*, Scheme 1, **1** and **4**) cause no toxic side effects (cardio-, hepato-, and myelotoxicity) at concentrations as high as 250 μM, and all xenografts receiving 3-days treatments survived and developed normally.

2. Results and Discussion

2.1 Synthesis and characterization of complexes

Rhenium complexes **1**-**8** were prepared according to the synthetic protocol illustrated in Scheme 1. Molecule **1** was obtained in high yield by treatment of the $[Et_4N]_2$*fac*-$[Re(CO)_3Br_3]$ salt with the 6-(bromomethyl)-2,2'-bipyridine ligand in a mixture of water and ethanol. Compounds **2-6** were prepared by nucleophilic substitution of the bromide atom of the α-diimine ligand of complex **1** by the corresponding amine. These complexes were prepared in moderate (*ca.* 40%) to good (>60%) yield following crystallization in a dichloromethane:pentane mixture. Compounds **7** and **8** were prepared respectively in an aqueous solution from the reaction of $[Et_4N]_2$*fac*-$[Re(CO)_3Br_3]$ with 0.5 and 1 equivalent of the bpy-DPA ligand which was in turn prepared according to a reported procedure [52].

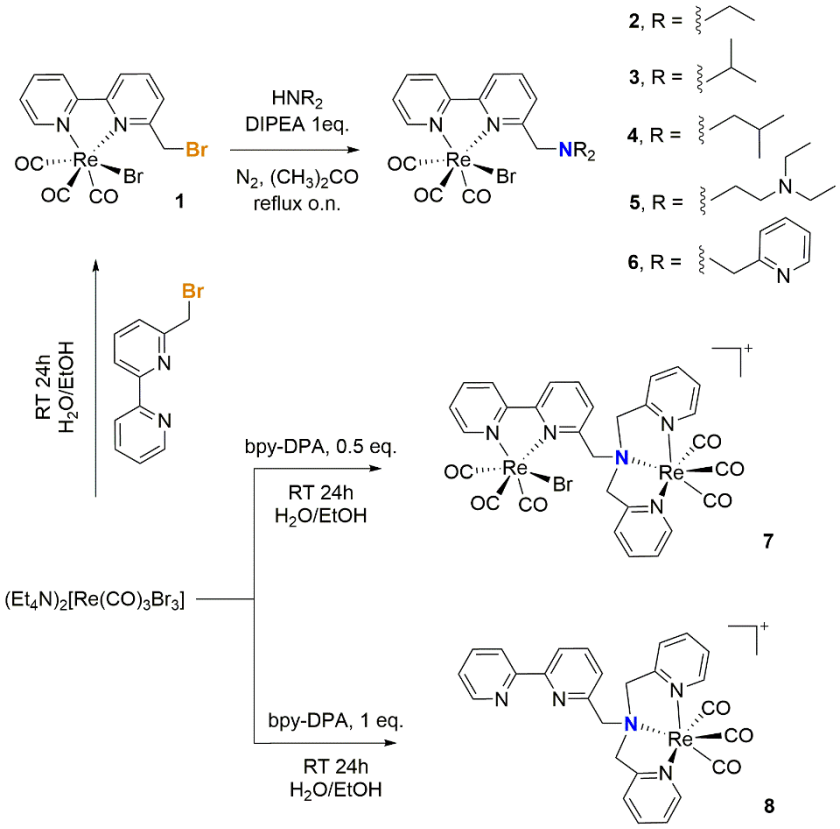

Scheme 1. Synthetic scheme for the preparation of complexes **1**-**8**.

^{1}H-NMR spectra (Fig. S1-S8) showed pure diamagnetic compounds, according to the symmetry given by the facial-arranged CO's and low-spin d6 nature of the metal ion. IR spectroscopy analysis was in accordance with the typical tricarbonyl vibration pattern.

Crystals suitable for x-ray diffraction analysis were obtained for five of the eight new species. Crystallographic details are presented in Table 1. Complexes **1**, **4**, **3** and **8** all crystallized in a monoclinic lattice and space groups *C*2/c, *P*21/n and *P*21/c (**3** and **8**) respectively, whereas **7** was obtained in the triclinic space group *P*-1 (Fig. 1). The five complexes all present a distorted octahedral geometry around the central metal ion but structural parameters are not significantly different from similar *fac*-$[Re(CO)_3]^+$ species (CCDC search).

Table 1. Crystallographic details for complexes **1**, **3**, **4, 7** and **8**.

	1	**3**	**4**	**7***	**8**
CCDC	1982188	1982189	1982190	1982191	1982192
Formula	$C_{14}H_9Br_2N_2O_3Re$	$C_{20}H_{23}BrN_3O_3Re$	$C_{22}H_{27}BrN_3O_3Re$	$C_{29.66}H_{23.66}Br_2N_5O_{6.67}Re_2$	$C_{26}H_{27}N_6O_9Re$
M_W	599.25	619.52	647.57	1089.04	753.73
T [K]	250(2)	250(2)	250(2)	250(2)	250(2)
Lattice	monoclinic	monoclinic	monoclinic	triclinic	monoclinic
Space group	*C*2/c	*P*21/c	*P*21/n	*P*-1	*P*21/c
Z	8	4	4	2	4
a [Å]	12.9334(8)	15.944(2)	15.9463(8)	8.4676(3)	12.6279(4)
b [Å]	11.2986(6)	10.6655(9)	10.5244(3)	12.5978(5)	17.1561(4)
c [Å]	22.2063(15)	13.2172(16)	16.1768(7)	17.7868(8)	13.2342(4)
α [°]	90	90	90	76.963(3)	90
β [°]	92.263(5)	100.188(10)	114.598(3)	85.213(3)	101.189(2)
γ [°]	90	90	90	72.830(3)	90
V [Å^3]	3242.5(3)	2212.1(4)	2468.50(19)	1765.80(13)	2812.63(14)
d_{calcd} [g/cm^3]	2.455	1.860	1.742	2.048	1.780
R_1, wR_2	0.0405, 0.0866	0.0624, 0.1462	0.0349, 0.0782	0.0511, 0.1219	0.0181, 0.0416

* a CH_3OH molecule with a 67% occupancy is present in the unit cell.

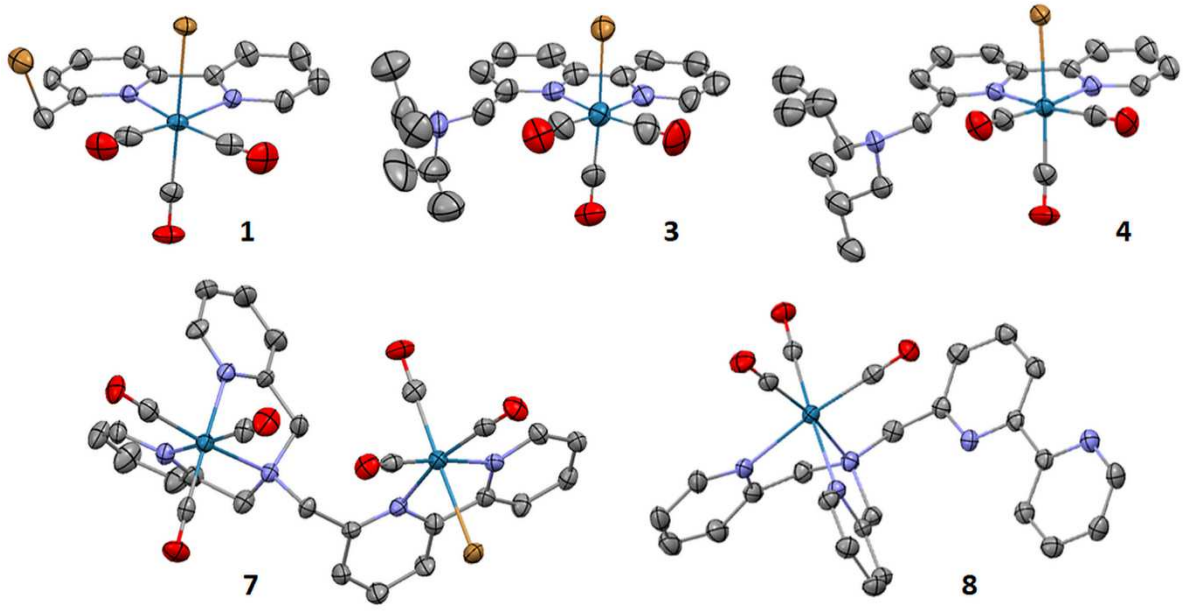

Figure 1. Crystal structures of compounds **1**, **3**, **4, 7** and **8**. Thermal ellipsoids are at 30% probability. Hydrogen atoms are omitted for clarity; for **7** one bromide and one methanol molecule and for **8** one nitrate and three water molecules are also omitted for clarity. Colour code: C, grey, O, red, N, light blue, Br, yellow, Re, turquoise blue.

2.2 Relative lipophilicity of complexes

The activity of drugs may often be correlated to their lipophilicity as it is generally the case for the cytotoxicity of Re(I) tricarbonyl complexes. The lipophilicity is defined by octanol-water partition coefficient (logP value) that can be determined by different experimental techniques [53, 54]. In order to define the relative lipophilicity of complexes **1**-**8**, we decided to calculate their molecular properties *via* the ALOGPS 2.1 and Molinspiration sowtwares [55, 56]. Results for the latter are given in Table 2. The values calculated by Molinspiration sowtware are not dissimilar to those experimentally determined for related complexes [57]. Both softwares indicate the same relative lipophilicity of the species, with the trend being similar to that of the α-diimine ligand only. Because of their primary coordination sphere, only complexes **1**-**6** can be directly compared. Their lipophilicity increases in the order **6** < **2** < **1** < **3** < **5** < **4** (**4** having the logP value of 5.12, Table 2). Overall, with the exception of their molecular weight, molecules rate well in the drug-likeness assessment (Table 2).

Table 2. Calculated molecular properties of investigated compounds for the assessment of drug-likeness.

Complex	miLogP[a] (Ligand)	TPSA[b]	N_{atoms}[c]	MW[d]	N_{ON}[e]	N_{OHNH}[f]	$N_{viol.}$[g]	$N_{rotb.}$[h]	Vol[i]
1	3.78 (2.22)	61.08	22	599.25[†]	5	0	1	1	289.13
2	3.63 (2.07)	64.32	26	591.48[†]	6	0	1	4	350.75
3	4.23 (2.66)	64.32	28	619.53[†]	6	0	1	4	383.93
4	5.12[†] (3.56)	64.32	30	647.59[†]	6	0	2	6	417.53
5	4.44 (2.88)	70.80	36	733.73[†]	8	0	1	12	510.26
6	3.34 (1.77)	90.10	36	717.60[†]	8	0	1	6	452.14
7	0.97 (1.77)	122.16	43	985.82[†]	11[†]	0	2	2	527.96
8	-0.87 (1.77)	90.10	35	635.68[†]	8	0	1	3	425.26

[a] Octanol–water partition coefficient (logP value obtained using Molinspiration method). [b] Molecular polar surface area in Å^2. [c] Number of nonhydrogen atoms. [d] Molecular weight. [e] Number of hydrogen-bond acceptors (O and N atoms). [f] Number of hydrogen-bond donors (OH and NH groups). [g] Number of "Rule of five" violations. [h] Number of rotatable bonds. [i] Molecular volume in Å^3. [†] "Rule of five" violation.

2.3 In vitro anticancer activity evaluation

The anticancer activity of *fac*-$[Re(CO)_3]^+$ compounds has been tested on several different cancer cell lines. The majority of the studies were focused on antiproliferative effects on cervical [30-33, 47, 51, 57-61], ovarian [62, 63], breast [12, 20, 25, 64-66] and epithelial adenocarcinoma [24, 49, 67, 68] cell lines showing IC_{50} values as low as e.g. 0.1 (HeLa) [30], 1 (MCF-7) [15], 0.75 (A549) [67], 4 (NB69 and H4 cells) μM [12]. To our knowledge, only a few rhenium(I) carbonyl complexes have been tested against colon cancer cell lines [16], [20, 69-75] (some of which are shown in Fig. 2), the majority of them revealing weak or no anticancer activity. Only *fac*-$[Re(CO)_3]^+$ complexes of pentylcarbonato (Re-2 and Re-3 in Fig. 2) and mono- and multinuclear Re-4 complexes demonstrated potent anticancer activity. The former resulting in an almost complete inhibition of CCL-227 colon cancer cells at a 4 μM concentration [69], while the latter (Re-4) were active on DLD-1 colon carcinoma cells with IC_{50} values between 10 and 18 μM, but mainly with a low selectivity index when compared to the effect on normal cells [71].

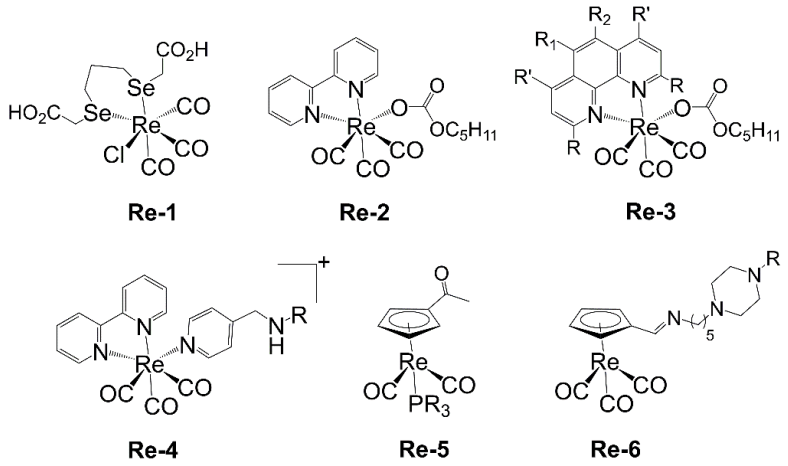

Figure 2. Selected structures of Re(I) carbonyl complexes tested against colon cancer cell lines.

In order to address the anticancer potential and selective activity towards carcinoma cells of newly synthesized complexes **1**-**8**, their antiproliferative effect was determined on a panel of cancer and normal cell lines (Table 3). As evident from Table 3, complexes **1-4** showed higher antiproliferative activity than complexes **5-8** (all but **5** bearing the 1-([2,2'-bipyridin]-6-yl)-N,N-bis(pyridin-2-ylmethyl)methanamine, bpy-DPA ligand), which conversely had weak or no cytotoxic effect on cancer cell lines and lung fibroblasts. Complexes **1-4** exhibited the highest potency against HCT-116 colorectal carcinoma cells and MIA PaCa-2 pancreatic carcinoma cells, with the IC_{50} values in the range of 5 to 10 μM (HCT-116) and 8 to 15 μM (MIA PaCa-2) range. Among them, **3** was the most active

compound on all the tested cancer cell lines except on HCT-116 cells; however, its equal or even higher toxicity towards healthy MRC-5 cells (Table 3) constrained it for further analysis. On the other side, complexes **1** and **4** showed moderate selectivity between healthy and cancer cell lines with Si of 6.8 and 3.2, respectively, while their toxicity *in vivo* was much lower (Table 3) making them suitable for further investigation. In comparison to other *fac*-$[Re(CO)_3]^+$ complexes tested against colon cancer cell lines, **1** and **4** are comparable to pentylcarbonato complexes [69] Re-2 and Re-3 (Fig. 2) and show greater antiproliferative activity than the other known rhenium(I) carbonyl complexes.

From a biological point of view, tumor cells response to various drugs depends on the unique properties of each cell line, including various pathways and signals, as well as inherent and acquired mechanisms of drug resistance (target modifications, overexpression of permeases or drug efflux transporters) [76]. Accordingly, distinctive characteristics of HCT-116 cells, including mutation in the KRAS proto-oncogene, stem cell-like properties, low differentiation level, fast division as well as epithelial morphology [77-79] could contribute to their higher sensitivity to the applied rhenium(I)-tricarbonyl complexes.

Table 3. *In vitro* cytotoxicity (IC_{50}, μM) and *in vivo* toxicity (LC_{50}, μM) of complexes **1**-**8**

Cells /Comp.	**1**	**2**	**3**	**4**	**5**	**6**	**7**	**8**
MRC-5	34±2	12.7±0.9	5±0.4	20±1	190±4	105±2	230±3	250±5
HCT-116	**5.0±0.2 (6.8)**	10.0±0.9 (1.3)	7.4±0.2 (0.7)	**6.2±0.1 (3.2)**	50±2 (3.8)	60±4 (1.8)	140±2 (1.6)	180±4 (1.4)
Mia PaCa-2	10.7±0.7 (3.2)	15±1 (0.8)	8.1±0.8 (0.6)	12±1 (1.7)	200±6 (1)	75±3 (1.4)	185±6 (1.2)	230±7 (1.1)
HeLa	27.5±0.9 (1.2)	17±1 (0.7)	5.0±0.3 (1)	9.5±0.8 (2.1)	143±2 (1.3)	70±4 (1.5)	190±5 (1.2)	200±7 (1.3)
A549	38±1 (0.9)	15.4±0.8 (0.8)	10 ±1 (0.5)	23.2±0.8 (0.9)	75±2 (2.5)	30±3 (3.5)	185±7 (1.2)	180±5 (1.4)
Zebrafish	244.4±10.2	<30	<30	271.4±4.8	>250	>250	261.2±9.7	>250

The values in brackets represent the selectivity index (Si) determined as a ratio between the IC_{50} values for MRC-5 cells and corresponding cancer cells. IC_{50} of compounds showing good selectivity towards HCT-116 colon cancer cells are **bold**.

2.4 In vivo toxicity assessment and therapeutic potential determination

Following *in vitro* anticancer activity assessment, the *in vivo* toxicity evaluation of compounds **1**-**8** was carried out using zebrafish (*Danio rerio*) embryos as the animal model system, with the aim to determine their therapeutic potential early in this study. In the current preclinical drug development pipeline, the zebrafish emerged as a versatile biotechnological platform for the toxicity assessment and bioactivity evaluation of chemically diverse molecules. Owing to their high genetic, physiological and immunological similarity to humans, and good correlation in response to pharmaceuticals, zebrafish markedly simplify the path to clinical trials and reduce the failure at later stages of testing [80, 81]. In last years, the preclinical toxicity of variety of metal complexes (Ag, Au, Ir, Os, Pt, Ru, etc.) has been tested in the zebrafish embryos [82-85], while, to the best of our knowledge, only one study explored Re(I) tricarbonyl complexes in this model [51].

Herein, according to the determined LC_{50} values (Table 3), active antiproliferative Re(I) complexes were ranked by toxicity as follow: **3** = **2** >> **1** > **4**. Among them, complexes **2** and **3** exerted toxic side effects at the doses ≥ 25 μM (especially cardiotoxicity), while **1** and **4** did not affect embryos survival, nor caused teratogenic malformations even at doses of 250 μM (Fig. 3). Notably, neither **1** nor **4** caused cardiac dysfunctions (pericardial edema, disturbed heart beating rate) (Fig. 3A, B) or myelotoxic response (neutropenia or inflammation) (Fig. 3E, F) at a concentration as high as 250 μM, nor induced the liver failure (reduced liver area index, hepatomegaly, liver necrosis or reduced yolk consumption) at 200 μM and 250 μM, respectively (Fig. 3C, D). On the other side, sunitinib and doxorubicin, two well-known anticancer agents, provoked severe pericardial edema, markedly decreased heartbeat rate, neutrophils occurrence, liver size as well as the liver area index (Fig. 3), which accompanied with the pronounced teratogenic malformations, led to embryos' death by 120 hours post-fertilization (hpf), as previously shown [83, 86].

Table 4. Therapeutic windows (Tw) of complexes **1**-**8**.

Cells/Compound	1	2	3	4	5	6	7	8
HCT-116	**48.9**	3.0	4.1	**43.8**	*5.0*	4.2	1.9	1.4
Mia Paca-2	**22.8**	2.0	3.7	**22.6**	1.3	3.3	1.4	1.1
HeLa	*8.9*	1.8	*6.0*	**28.6**	1.8	3.6	1.4	1.3
A549	*6.4*	2.0	3.0	*11.7*	3.3	*8.3*	1.4	1.4

The Tw values in the range from 5 to 20 are *italic*, while those above 20 are **bold**.

Herein, we could not determine a trend of the *in vivo* toxicity of complexes **1**-**4** as a function of their lipophilicity. Extensive literature data show a strong correlation between compound's lipophilicity (logP) and their uptake by zebrafish embryos, proving that lipophilic molecules are uptaken up by the embryos [87], which is a very important for their *in vivo* efficiency and toxicity evaluation. On the other side, the meta-analysis of toxicity of various compounds from diverse chemical classes in the zebrafish model proved no correlation between the compounds' toxicity and lipophilicity (logP) [88, 89], what we have also observed in this study.

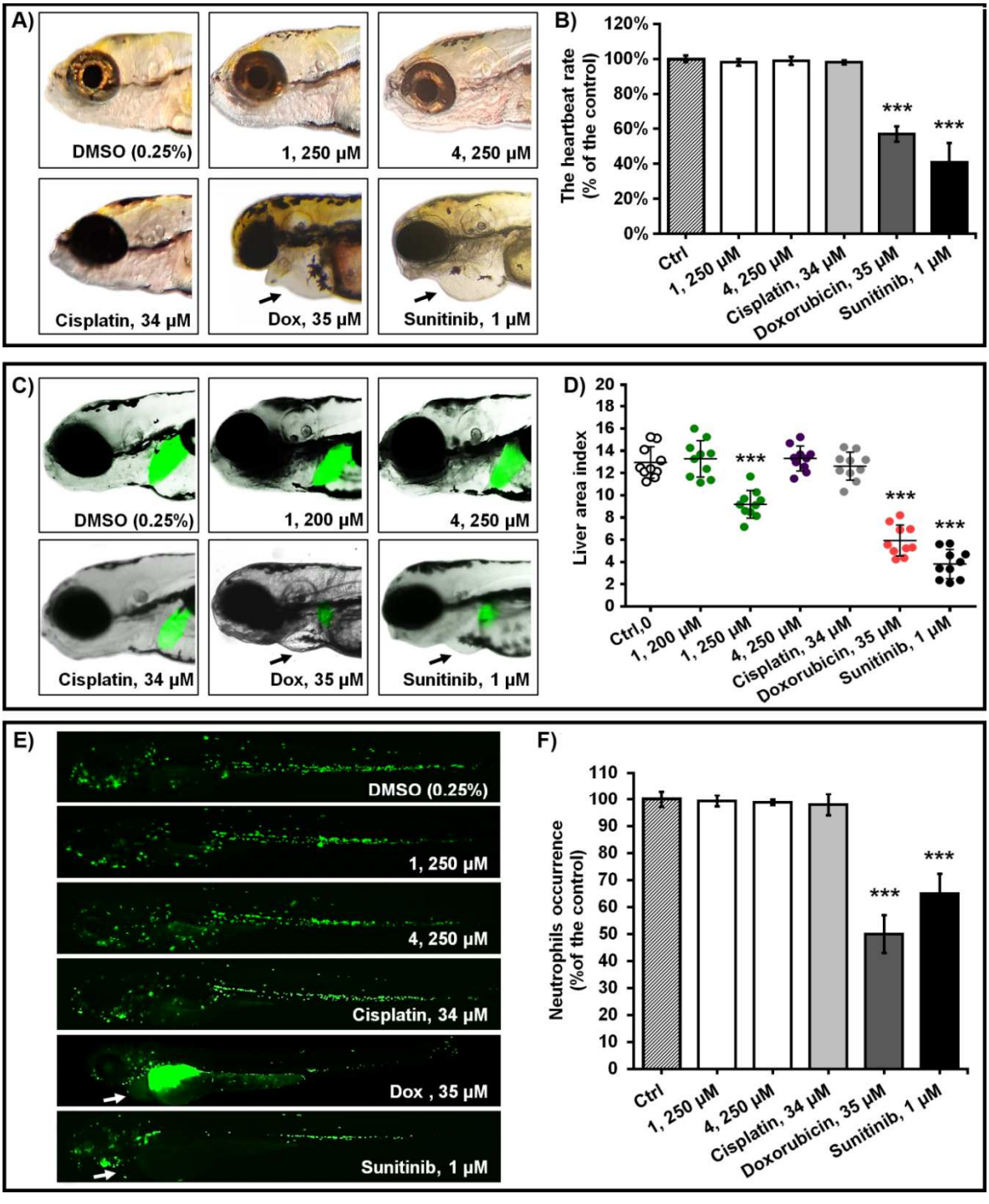

Figure 3. Complexes **1** and **4** are not cardio-, hepato- or myelotoxic in the zebrafish model. Cardiotoxicity was addressed in wild type (wt) embryos (n = 30) according to the appearance of pericardial edema (arrow) (A) and decreased heart beating rate (B). Hepatotoxicity was assessed in *Tg(-2.8fabp10a:*EGFP) embryos with fluorescently labelled liver (n = 10) according to the liver fluorescence (C) and the liver area index (D), while myelotoxicity was evaluated in *Tg*(*mpx*:GFP) embryos with fluorescently labelled neutrophils (n = 30) according to neutrophils fluorescence (E) and occurrence (F). All toxicity endpoints analysed in the zebrafish embryos treated with **1** and **4** were compared to those in the control (DMSO-treated) group and the groups treated with clinically approved drugs - cisplatin, doxorubicin and sunitinib malate. Complexes **1** and **4** did not provoke any side effect at doses up to 250 μM (except hepatotoxicity of **1** at 250 μM). Cisplatin, sunitinib and doxorubicin appeared to be cardiotoxic, hepatotoxic and myelosupressive at the tested concentrations. $P < 0.05$; $^{**}P < 0.01$; $^{***}P < 0.001$.

Since cardio-, hepato- and immunotoxicity are the most commonly encountered drawbacks of clinically approved anticancer drugs, limiting their long-term application in chemotherapy, data obtained in this study indicate a very good toxicity profile of complexes **1** and **4**, which could be considered as safe agents with promising anticancer activity. Furthermore, we found that both molecules possess a large therapeutic window (determined as the LC_{50}/IC_{50} ratio), greater than 43 (Table 4), what is of particular relevance since HCT-116 present a CRC cell line that easily acquires resistance to clinical anticancer drugs, including cisplatin, oxaliplatin, docetaxel, 5-FU, and others [79, 90-92]. Taken together, these results prompted us to further address the efficacy of **1** and **4** against colorectal carcinoma *in vivo*. We evaluated both anticancer and anti-angiogenic activity of these molecules using various zebrafish models.

2.5 Inhibition of angiogenesis in vivo

Angiogenesis (new vessels formation) is an essential process for tumour growth, invasion and metastasis [93]. Since CRC are highly vascularized and metastatic tumours, the increased angiogenesis in CRC is associated with poor prognosis and tumour relapse [94]. Accordingly, inhibition of tumour vascularization is a proven clinical strategy for CRC treatment [3], where the combination of anti-angiogenic drugs with cytotoxic drugs increases anti-tumour efficacy and provides significantly better survival of the cancer patients [3, 95]. Compared to conventional chemotherapy with cytostatic agents, a treatment targeting

angiogenesis brings relatively less side effects associated with prolonged administration and less risk of developing tolerance because such treatment is focused on vascular cells.

To the best of our knowledge, the anti-angiogenic potential of rhenium tricarbonyl complexes remains mostly unexplored, in contrast to complexes of other third row transition metals like gold, osmium, and iridium [44, 83, 96, 97]. Yang *et al*. [98] recently reported a theranostic rhenium(I) tricarbonyl-dichloroacetate conjugate, which at a dose of 5 μM destroyed already formed vasculature in zebrafish embryos, leading to their death within 48 h post-treatment. To address whether complexes **1** and **4** possess anti-angiogenic activity, *Tg*(*fli1*:EGFP) zebrafish embryos with GFP-labelled endothelial cells were challenged to different doses of both compounds for 24 h, and imaged by fluorescent microscopy to directly visualize the effect of the applied agents on new vessel development. In normally developing embryos, 5-9 subintestinally vessels (SIVs) and 28-30 intersegmental vessels (ISVs) connected with dorsal lateral vessels (DLAVs) were present, while the anti-angiogenic phenotype is defined by reduced number/length of ISVs or disrupted DLAVs.

We found that complexes **1** and **4** are highly effective in inhibition of angiogenesis. They were active at very low doses and in a dose-dependent manner, and the treated embryos displayed the anti-angiogenic phenotype already at 0.25 μM and 0.5 μM doses, for **1** and **4** respectively (Fig. 4, χ^2 test). We point to the fact that the overall anti-angiogenic effect of both Re(I) tricarbonyl complexes exceeded that of sunitinib, a clinical anti-angiogenic drug. At 1 μM, sunitinib reduced subintestinal vessels (SIVs) and intersegmental vessels (ISVs) length by 50.4 ± 2.1 % and 41.2 ± 1.7 %, respectively, while complex **1** showed higher inhibitory effect than this drug decreasing the SIVs angiogenesis by 57.6 ± 1.9 % ($P < 0.001$) and the ISV angiogenesis by 49.1 ± 2.6 % ($P < 0.001$) (Fig. 4 C, D), and complex **4** exerted comparable activity to 1 μM sunitinib at the doses of 2 μM and 2.5 μM, respectively. Moreover, when applied at the doses ≥ 3 μM, the overall antivascular effect of **1** and **4** was much greater than that of 1 μM of sunitinib, achieving by 100% regression in ISVs and SIVs length ($P < 0.001$). In addition, the investigated Re(I) complexes exerted much higher anti-angiogenesis potency than that reported for auranofin, a gold-based agent [83].

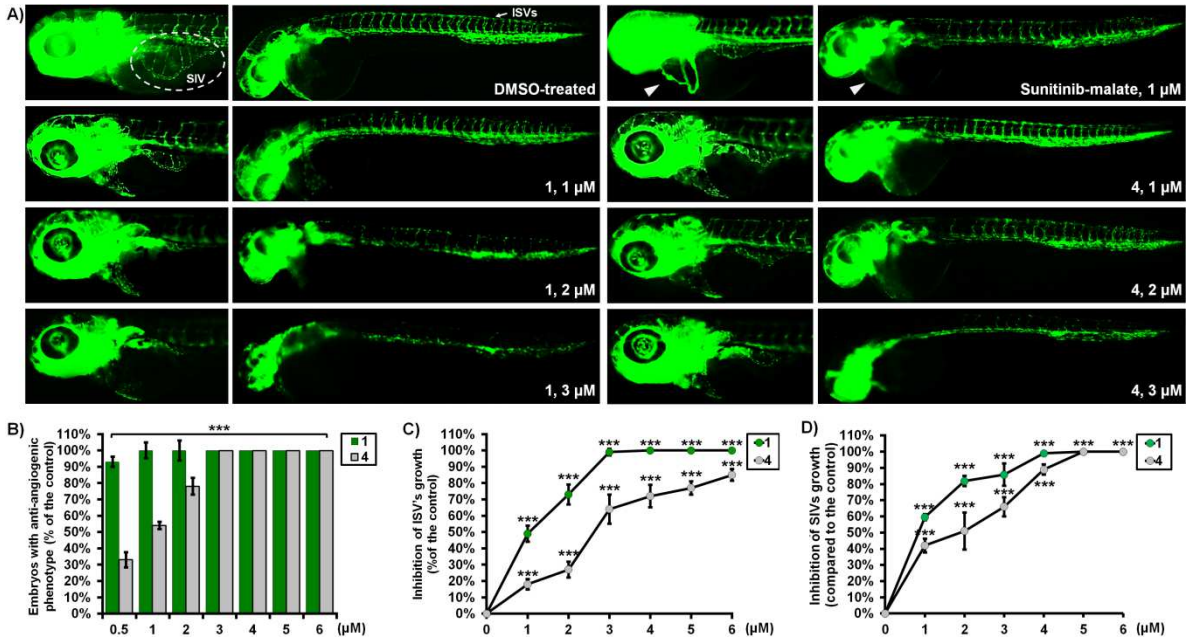

Figure 4. Complexes **1** and **4** effectively inhibited angiogenesis in *Tg*(*fli1*:EGFP) zebrafish embryos with fluorescently labelled endothelial cells (n = 30). Embryos were exposed to different doses of **1** and **4**, and evaluated for the inhibition of the ISV and the SIV vasculature at 48 hpf and 72 hpf, respectively. At 1 μM, the inhibitory activity of compound **1** was greater than that of clinical anti-angiogenic drug sunitinib. The latter, however, was cardiotoxic at the effective dose, while **1** did not elicit any toxic response in the treated embryos. Compound **4** at a dose of 3 μM displayed comparable activity to sunitinib at 1 μM, and, as **1**, caused no side effects. Representative images of embryos are shown.

It is important to emphasize that the treatments with effective doses of **1** and **4** elicited no toxic response in zebrafish embryos, while sunitinib applied at anti-angiogenic doses ≥ 1 μM provoked life-threatening pericardial edema (Fig. 4A) and markedly reduced the heartbeat rate ($P < 0.001$) what progressively decreased the embryos' survival by 120 hpf. These toxicity issues have restricted the application of sunitinib at higher doses and its overall anti-angiogenic potential. Cardiotoxicity, in particular, is one of the major obstacles for a long-term use of many clinical anti-angiogenic drugs, including sunitinib [99].

To determine the overall therapeutic anti-angiogenic potential of **1** and **4**, and whether these compounds have more specific inhibitory effects on neovascularization in comparison to toxicity/teratogenicity, we determined their IC_{50ang} doses (the concentration upon which 50% of embryos displayed anti-angiogenic phenotype), EC_{50} doses (the effective concentration resulting in toxic response at 50% of embryos) and therapeutic windows (Tw; the ratio between EC_{50} and IC_{50ang} values). The therapeutic potential of complexes was evaluated in relation to sunitinib and results are given in Table 5. The data show that IC_{50ang}

doses of **1** and **4** are far below their respective EC_{50} doses, contrary to that of sunitinib, for which EC_{50} and IC_{50ang} doses are close to each other, indicating thus high risk of fetal toxicity [100]. Based on the respective Tw values, **1** and **4** displayed 349-fold and 211-fold higher anti-angiogenic potential than this FDA-approved drug (Tw = 1.41), implying their possible use as effective and safe anti-angiogenic agents in oncological practice.

Table 5. Toxicological parameters derived from the concentration-response curves for the toxicity assessment and anti-angiogenic potential of complexes **1** and **4** in comparison to the clinical drug sunitinib malate.

Treatment	LC_{50}	EC_{50}	IC_{50ang}	Tw	EC_{50}	
					ISVs	SIVs
1	244.4	244.4	<0.5	>488.8	1.6	0.9
4	271.4	271.4	0.9	295	2.6	2.1
Sunitinib	1.1	0.7	0.5	1.4	1.8	1.1

LC_{50} – the concentration inducing the lethal effect of 50% embryos, EC_{50} – the concentration affecting 50% embryos (survival and developmental defects), IC_{50ang} - the concentration upon which 50% of embryos displayed anti-angiogenic phenotype, Tw – therapeutic window determined as the EC_{50}/IC_{50ang} ratio, EC_{50} (ISVs) - the effective concentration resulting in 50% decrease ISVs length compared to the control (DMSO-treated) group. LC_{50}, EC_{50}, IC_{50ang} and EC_{50} (ISVs or SIVs) values are expressed in μM.

2.6 Anticancer activity in the zebrafish xenograft model of colorectal carcinoma

The potent antiproliferative activity of complexes **1** and **4** (Tables 3, 4) accompanied with the effective inhibition of angiogenesis (Fig. 4) fortified us to evaluate them against colorectal carcinoma *in vivo*. To date the anticancer activity of Re(I) tricarbonyl complexes has rarely been evaluated *in vivo*. To our knowledge, only three studies have reported the efficiency of *fac*-$[Re(CO)_3]^+$ complexes in animal models of human tumors. Collery *et al.* have reported a very promising Re(I) diselenoether complex candidate for breast-tumor treatment, which completely inhibits tumor development in MDA-MB-231-bearing mice xenografts, but it is inactive in lung and colorectal carcinoma cell lines [17, 101]. More recently, Konkankit [62] and He [68] described *fac*-$[Re(CO)_3]^+$ complexes with 1,10-phenthroline and β-carboline derivatives, respectively, which induced up to 60% regression of ovarian or lung tumors in carcinoma mice models. So far, none of the *fac*-$[Re(CO)_3]^+$ complexes with the reported anticancer activity against CRC cell lines has been evaluated *in vivo* in animal tumor models.

Herein, we investigated the activity of complexes **1** and **4** against human colorectal carcinoma *in vivo* using the zebrafish-HCT-116 xenograft model. Zebrafish xenografts has

emerged in last years as a new platform for translational research in human carcinomas demonstrating crucial hallmarks of cancer biology, such as tumour cells proliferation, dissemination, metastasis and tumour angiogenesis, and providing differential discrimination in anticancer therapy responses with single-cell resolution [102, 103]. Accordingly, HCT-116 cells were fluorescently labelled and injected into the yolk of *Tg*(*fli1*:EGFP) embryos, and at 3 days post injection (dpi), xenografts were processed for fluorescence microscopy evaluating the effects of applied complexes on the tumour mass development, tumour neo-angiogenesis, as well as cancer cells dissemination and metastasis.

Our results (Fig. 5) show that treatments with **1** and **4** significantly inhibited both colorectal tumour growth ($P < 0.001$) and cancer cells dissemination ($P < 0.001$), the complexes being noticeably effective even at a concentration 8-fold lower of their respective *in vitro* IC_{50} values (Table 3). By determining the $ED_{50\text{-}HCT116}$ values (effective drug concentration reducing tumour mass by 50% in relation to that in untreated xenografts) we found that **1** exerted 2.3-fold higher anticancer potency than **4** ($ED_{50\text{-}HCT116}$ of 1.23 µM vs. 2.81 µM). Comparison of tumour growth to untreated HCT-116 xenografts at 3 dpi (120 hpf) indicated that **1** and **4** reduced tumour mass in the treated xenografts by 38.2 ± 5.18% and 41.2 ± 9.11% at 1/8 × IC_{50} doses, respectively ($P < 0.0001$, for both compounds), while tumors almost completely disappeared upon ½ × IC_{50} doses of complexes (corresponding to 2.5 µM and 3.1 µM, respectively, Fig 5B).

In addition to the anti-tumor effect, dissemination of HCT-116 cells was significantly reduced already at 1/8 × IC_{50} doses of **1** and **4** ($P < 0.001$, for both compounds), and completely abolished at higher doses (Fig. 5C, D). Moreover, complexes efficiently suppressed tumor neo-angiogenesis in a dose-dependent manner ($P < 0.001$), preventing ectopic vessels formation from the SIV basket, especially at ½ × IC_{50} doses (Fig. 6C, D), in contrast to relatively robust angiogenic response in untreated HCT-116 xenografts (Fig. 6A). It is well known that HCT-116 cells injected close to the SIV basket release pro-angiogenic factors locally, and thus change normal developmental pattern of SIVs by stimulating the endothelial cells migration and the growth of sprouting vessels towards the implant [104]. Unlike the complexes, cisplatin appeared inactive against grafted CRC cells since it failed to inhibit tumour development and HCT-116 cells dissemination at its maximal non-toxic dose of 34 µM (Fig. S13), and decreased the ectopic vessels length only in few treated embryos (Fig. 6B), in line with study of Stenton [105].

As stated above, the size of HCT-116 tumors was markedly reduced in xenografts receiving 1/8 × IC_{50} doses of complexes, as compared to untreated group. Initially, tumor

cells were injected and developed into the yolk (120 hpf, 3 dpi), an environment rich in nutrients. The ISV and the SIV vasculature of these xenografts stayed functional and visible during entire treatment (Fig. 5A), enabling thus additional nutrients perfusion to HCT-116 cells and their dissemination for a period of three days post injection (treatment). Considering that: a) tumor mass was reduced in all xenografts receiving 1/8 × IC_{50} doses (~40%; Fig. 5B); b) ~60% of these xenografts still had ectopic vessels for HCT-116 cells dissemination (Fig. 6D); c) metastases occurred only in 16% (complex **1**) and 36% (complex **4**) of embryos (Fig. 5C) and at a very low number (1-5 cells per embryo) (Fig. 5D); we suggest that the anti-tumor and antimetastatic effects of **1** and **4** can be initially assigned to their cytotoxic activity on HCT-116 cells, while at higher doses, this activity is accompanied with inhibition of tumor neo-vascularization and results in markedly decreased tumor growth. These findings are in a line with the potential of complexes to inhibit new vessel formation in the angiogenesis assay (Fig. 4), and indicate their no detrimental effect on already established vascularization [106].

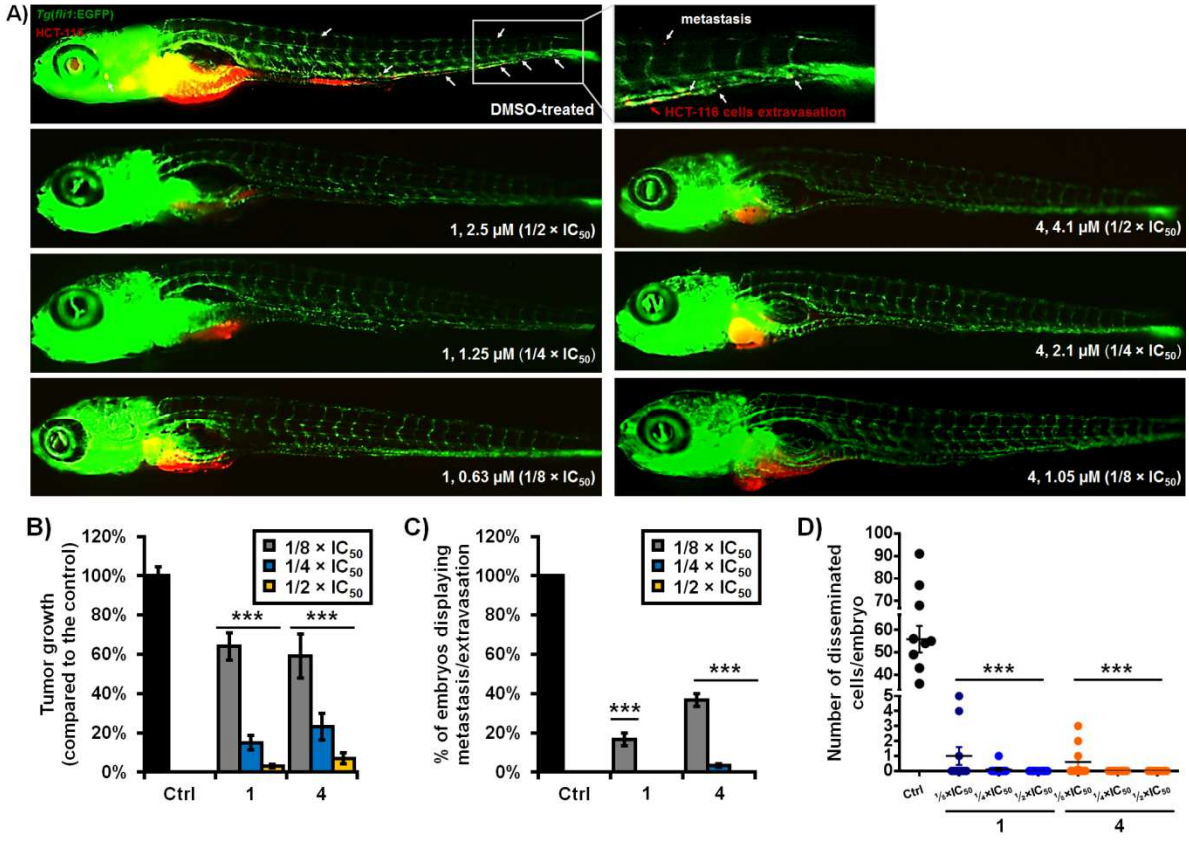

Figure 5. Anticancer activity of complexes **1** and **4** against highly metastatic human HCT-116 cells in zebrafish xenografts. *Tg*(*fli1*:EGFP) xenografts (n = 20) were exposed to complexes **1** and **4** at doses corresponding to their respective 1/8 × IC_{50} - 1/2 × IC_{50} values, and analysed after 3-days treatments for tumour progression and metastasis. Representative

fluorescent microscopy images are shown (A); white solid arrows indicate disseminated cells. The applied treatments markedly reduced the tumor growth (B), incidence of cancer cells dissemination (C) and the number of disseminated HCT-116 cells per xenograft (D) compared to those in the control group ($P < 0.001$, for all hallmarks). Data are normalized in relation to the control group (B, C). *$P < 0.05$; **$P < 0.01$; ***$P < 0.001$.

In addition to the anti-tumor activity attained *in vivo*, it is important to note that after 3-days treatments all xenografts survived and developed without side effects (Fig. 5A). Cardiovascular toxicity, induced by different mechanisms such as mitochondrial dysfunction, DNA damage in cardiomyocytes, damage of heart endothelial cells [107], is one of the most common drawbacks of neoplastic drugs. In our study, we did not observe any signs of cardiac dysfunction (edema, hypo/hypertension) or a decrease of endothelial cells fluoresce in the pericardium of treated xenografts.

The tested Re(I) tricarbonyl complexes exerted much higher anticancer activity in the zebrafish-human CRC cells xenografts than on the cancer cells in culture, implying that overall therapeutic potential of **1** and **4** against colorectal carcinoma is higher *in vivo* than what we expected from *in vitro* assay. Various factors may account for this discrepancy, including e.g. tumor cells density, duration of *in vitro* treatments, number of injected tumor cells in embryos, site of their injection and duration of *in vivo* treatment. In addition to the direct antiproliferative effect of Re(I) complexes on the implanted HCT-116 cells and a possible effect on the tumor microenvironment, the high efficacy in restricting tumor growth in xenografts could be attributed to the activity of their innate immune cells, especially of neutrophils. A study of Collery demonstrated the importance of preserving immunity for the anticancer activity of Re-diselenoether complexes since the investigated complex was completely ineffective if mice were pre-treated with irradiation [17]. The importance of neutrophils in determining the efficacy and toxicity of clinical anticancer therapies has become increasingly apparent over the past decade [108]. Neutrophils are predominant immune cells that protect the host from microbial infection, and their roles in tumor have long been ignored due to their short life span and terminal differentiation phenotype. Recent studies have shown that neutrophils make up a significant portion of the inflammatory cell infiltrate in cancer, whereby they show high functional plasticity and display both antitumor and pro-tumor activities. Moreover, the number of neutrophils in blood and tumor tissues of cancer patients is associated with disease progression and patient outcome. From the one side, anti-tumor neutrophils (N1 neutrophils) eliminate malignant cells by releasing the cytotoxic contents in their granules (reactive oxygen species - ROS, myeloperoxidase,

hydrogen peroxide, and proteases) or secreting immune mediators to recruit and activate other antitumor effector cells [109]. On the other side, tumor derived factors released within the tumor environment can convert anti-tumor neutrophils into a pro-tumor neutrophils (N2 phenotype) which promote the proliferation, migration, and invasion of tumor cells, and stimulate angiogenesis. Accordingly, to preserve neutrophils during chemotherapy is very important for microbial infection defence, while preventing the switch of the anti-tumor into the pro-tumor phenotype could be an important strategy for an effective anti-tumor therapy [108, 109]. Herein, our finding that Re(I) tricarbonyl complexes **1** and **4** did not provoke neutropenia in zebrafish embryos over 5-days treatments (unlike other cytostatics of clinical relevance, Fig. 3C, D) is of a particular significance, especially due to the fact that neutropenic cancer patients are highly susceptible to microbial infections [110].

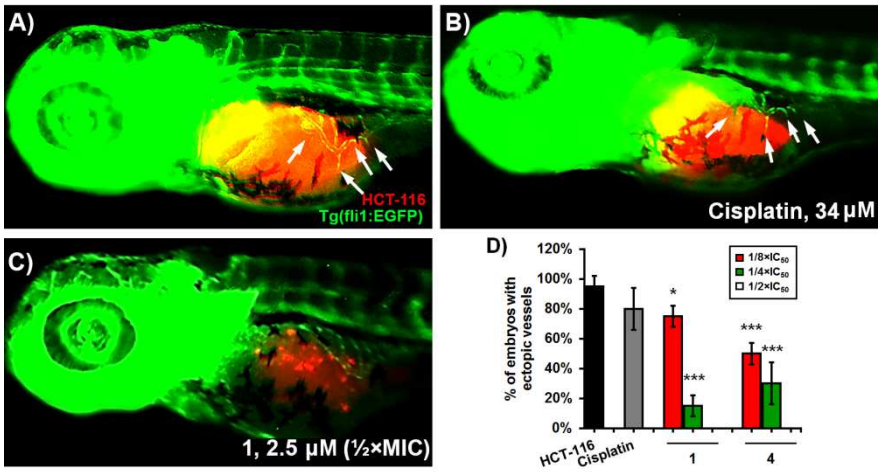

Figure 6. Inhibition of tumor-induced neoangiogenesis in the zebrafish xenografts bearing HCT-116 tumors. Lateral views of the transgenic *Tg*(*fli1*:EGFP) embryos at 72 hpf (24 hpi) showing the ectopic vessels (arrow) sprouting from the SIV plexus upon stimulation by closely injected HCT-116 cells (A-C). Newly formed ectopic vessels in untreated (A) and cisplatin-treated xenografts (B) are denoted, while vessels were no formed upon treatment with complex **1**. (D) Dose-dependent inhibition of neovascularization by complexes **1** and **4**, and cisplatin at its the highest safe dose of 34 µM. Scale bar =100 µm.

2.7 Cellular localization and interaction of 1 and 4 with nucleobases and amino acids.

It is generally accepted that for rhenium-based anticancer agents to exhibit their antiproliferative properties, they have to be internalized into the cell. In order to provide preliminary indications of possible target sites and mechanism of action of complexes **1** and **4**, we first investigated their distribution within HCT-116 cells by fluorescent microscopy. The complexes exhibit weak fluorescence with maximum emission wavelength (λ_{em})

centered at 624 and 606 nm, respectively (for **1** and **4**, maximum exctitation wavelength (λ_{ex}) was 400 nm, Fig. S12). Fluorescent microscopy investigation of HTC-116 cells incubated with **1** and **4** at 4 °C showed no fluorescent signal detection, contrary to the fluoresce visible in cells incubated at 37 °C, suggesting that the internalization of the investigated complexes across the membrane may occur *via* an energy-dependent process [60, 111, 112]. The intracellular localization of the complexes was further probed by determing the colocalization of their fluorescence with organelle-specific fluorescent probes. As shown in Fig. 7, complexes **1** and **4** were distributed in the cytoplasm of HCT-116 cells (visible as blue diffuse emission over the whole cell), while the nuclei showed very weak or no emission in contrast to strong staining with DAPI (Fig. 7a, a', c and c'). In addition to cytosolic distribution of **1** and **4**, co-staining experiment with LysoTracker Deep Red dye showed that the complexes were parially localized in the lysosomes, being apparent as large perinuclear cytoplasmic vesicles (Fig. 7b', b'', d' and d'').

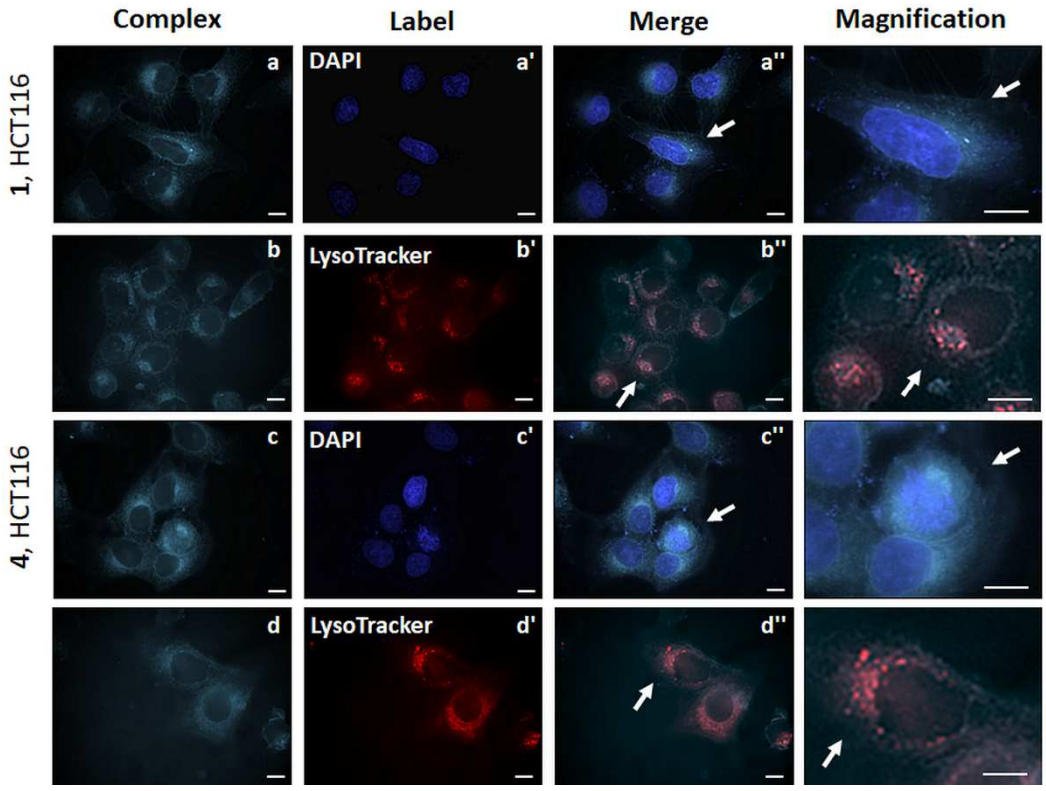

Figure 7. Fluorescent microscope images of HCT-116 cells treated with **1** and **4** (5 µM, 30 min, 37 °C/5% CO_2). The intracellular distribution of complex **1** (a and b) and complex **4** (c and d), as well as of DAPI-labelled nuclei (a' and c') and LysoTracker-labelled lysosomes (b' and d'). The co-localization of the applied complexes with DAPI or LysoTracker dye is shown on images a'' - d''. Arrows indicate magnified cells in the last column. Magnifications × 100 was used. Scale bars = 10 µm.

Such cytosolic-lysosomal distribution of the rhenium(I) tricarbonyl complexes has previously been reported in molecules bearing β-carboline [68], 1,10-phenanthroline [49, 113] and diimine ligands [57]. Preferential accumulation in lysosomes, mitochondria or localization only in cytoplasm has also been evidenced for other rhenium(I) tricarbonyl molecules [114, 115]. It is noteworthy to point out that the lysosomes are emerging as very attractive targets in anticancer therapy, and drugs affecting the integrity of lysosomes have been proven to be effective in cancer treatment [116-120].

Due to the fact that the fluorescence of **1** and **4** is visible throughout the entire cytosplasm of HCT-116 cells, it is possible that some cytosolic proteins could be targets of the tested molecules, as recently demonstrated for a Re(I) tricarbonyl isonitrile complex which exerted anticancer activity *via* the endoplasmic reticulum stress and the accumulation of misfolded proteins [113]. Accordingly, we probed the reactivity of complexes **1** and **4** with hen egg white lysozyme (HEWL), a model protein often employed to investigate metal–protein adducts [121-127]. The interaction of the complexes with HEWL was examined by HPLC and ESI-MS. Similar rhenium complexes have been previously shown to preferentially bind to the only histidine residue of the enzyme (His15) giving e.g. *fac*-[His15-$Re(CO)_3(X)_2$] type adducts [128-130]. Complex **4** showed no binding to HEWL. On the other hand, ESI-MS analysis of the interaction of **1** with HEWL revealed, already after 1 day of incubation, the formation of a new lysozyme-complex adduct with a mass increased by 440 mass units (Fig. S14). This mass correspond to complex **1** lacking two bromides. The adduct is consistent with the possibility that **1** may have alkylated HEWL by reacting with the amine groups of basic amino acids (aa) residues of e.g. lysine, arginine, asparagine or glutamine (collectively 35 aa of the 129 composing the protein), *via* the same nucleophilic substitution of the bromide atom of the α-diimine ligand as shown in Scheme 1. We cannot exclude the possibility of His15 coordination, however, lack of direct His15 binding of *fac*-[$Re(CO)_3(L^2)Br$] complexes (L^2 = bidentate ligand) was consistently observed in previous studies [128, 131]. In order to confirm aa alkylation by **1**, we further tested the reactivity of the complexes with Fmoc-protected Lys-OH, Asn-OH and Gln-OH (all bearing unprotected side chains). Complexes **1** and **4** showed no interaction with Asn and Gln, but **1** clearly alkylated the side chain Fmoc-Lys-OH (Fig. S15). In addition to that, both metal species showed unspecific interaction with Fmoc-Lys-OH (i.e. $-NH_2$ or $-COO^-$ coordination to rhenium, Fig. S15-S16).

The lack of clear evidence of nuclear accumulation of **1** and **4** does not exclude the possibility that a small fraction of the complexes enters the nucleus or that the same may

exert their cytotoxicity *via* DNA or RNA interactions or nucleobases binding. Several *fac*-$[Re(CO)_3]^+$ are shown to bind to nucleobases and double stranded (ds) DNA [57, 132-139]. Therefore, we probed next the reactivity of the complexes with ds lambda bacteriophage DNA (λ-DNA) and the model nucleobases adenine and guanine. Gel electrophoresis experiments revealed that only **1**, and only at concentrations > 250 μM, significantly prevented ethidium bromide intercalation in λ-DNA (Fig. S17). Furthermore, ^{1}H NMR spectroscopy provided no evidence of adenine or guanine coordination to the metal center (Fig. S18-S19). Collectively, the results indicate that DNA is an unlikely target for the mode of action of **1** and **4**. The complexes, therefore, are likely to act at the cytoplasmatic level by altering key cellular processes possibly *via* alkylation of one or several proteins (complex **1**).

3. Conclusions

We have reported the synthesis, characterization and the evaluation of a small library of rhenium(I) tricarbonyl complexes for anticancer activity, and discovered two complexes, **1** and **4,** as promising agents against CRC with a good therapeutic profile. These two complexes are found to possess triple anticancer, anti-angiogenic and antimetastatic activity *in vivo,* not yet reported for a *fac*-$[Re(CO)_3]^+$ molecule, being effective in the range of low doses from 1 to 3 μM. The novel rhenium(I) tricarbonyl complexes displayed up to 349-fold higher anti-angiogenic potential than clinical drug sunitinib malate, while in the zebrafish xenograft model of colorectal carcinoma achieved almost complete inhibition of tumour growth, tumor vascularization and tumor cells metastasis, contrary to cisplatin. Moreover, the investigated complexes showed a large therapeutic window and at doses as high as 200-250 μM did not induce toxicity issues encountered in clinical anticancer drugs (cardio-, hepato-, and myelotoxicity), appearing to be much safer and more effective than FDA-approved sunitinib, doxorubicin or cisplatin, and demonstrating a strong potential for the application in CRC therapy. *In vitro* co-localization studies suggested that the investigated complexes localize preferentially in the cytoplasm, and, to some extent, within the lysosomes and may act by altering cellular processes possibly *via* alkylation of one or several key proteins. Future efforts will be directed towards studies aimed at verifying anti-tumour efficacy and therapeutic potential of the molecules on primary tumor cells from the patients with CRC and the detailed elucidation of their targets and mechanism of action.

4. Materials and Methods

4.1 Reagents and chemicals.

All reagent and solvents were purchased from sigma Aldrich and TCI and used without further purification. 6-(bromomethyl)-2,2'-bipyridine ligand was synthesized from commercially available 2,2'-bipyridine [140]. Ligand 1-([2,2'-bipyridin]-6-yl)-N,N-bis(pyridin-2-ylmethyl)methanamine (DPA-bpy) was synthesized following the procedure of Radaram *et al.* from 6-(bromomethyl)-2,2'-bipyridine and commercially available dipicolylamine [52]. The $[Re(CO)_3Br_3](Et_4N)_2$ salt was synthesized from dirhenium decacarbonyl in two steps following the procedure of Alberto *et al.* [141].

4.2 Instruments and analysis.

NMR spectra were measured on a Bruker Advance III 500 or 400 MHz. The corresponding ^1H chemical shifts are reported relative to residual solvent protons. Mass analyses were performed either using ESI-MS on a Bruker FTMS 4.7-T Apex II in positive mode or MALDI with a Bruker UltrafleXtreme MALDI-TOF. UV-Vis spectra were measured on a Jasco V730 spectrophotometer. IR spectra were recorded on a Perkin Elmer FTIR Frontier Serie 99155 equipped with a PIKE TECHNOLOGIES Glad-iATRTM system. Preparative and analytical HPLCs were performed with a Merck Hitachi Hitachi L-7000 system, which comprises a Pump L-7100 and a UV-Detector L-7400. For preparative HPLC, a column Macherey-Nagel Nucleodur C18 HTec (5 µm particle size, 110 Å pore size, 250 × 21 mm) was used. Aqueous trifluoroacetic acid 0.1% solution and pure methanol were respectively used as solvents (A) and (B). The compounds were separated using the following gradient: 0–5 min (75% A), 5–35 (75% A → 0% A), 35–45 min (100% B) or 0–5 min (50% A), 5–30 (50% A → 0% A), 30–45 min (100% B), the flow rate set to 5 mL min^{-1} and the compounds detected at 320 nm. Single crystal diffraction collections were done on Stoe IPDS2 diffractometer ($MoK\alpha_1$ (λ = 0.71073 Å)) equipped with a cryostat from Oxford Cryosystems. The structure were solved with the ShelXT structure solution program **[142]** using Intrinsic Phasing and refined with the ShelXL refinement package **[143]** using Least Squares minimisation. All the crystal structures are deposited at the Cambridge Crystallographic Data Centre. CCDC numbers 1982188 to 1982192 contain the supplementary crystallographic data for this paper. These data can be obtained free of charge from the Cambridge Crystallographic Data Centre *via* www.ccdc.cam.ac.uk/structures. The purity of the synthesized materials was determined to be ≥ 95% by RP-HPLC analysis.

579 ***4.3 General synthesis procedures.***

580 ***fac*-[Re(CO)$_3$L$_2$Br] (L$_2$ = 6-(bromomethyl)-2,2'-bipyridine), 1.** To a stirring 50 mM
581 solution of [Re(CO)$_3$Br$_3$](Et$_4$N)$_2$ in water (850 mg in 22 mL H_2O) a 450 mM solution of
582 6-(bromomethyl)-2,2'-bipyridine (0.9 eq.) in ethanol (247 mg in 2.2 mL EtOH) was added.
583 The resulting mixture was stirred two days at room temperature (RT) after which time a
584 yellow precipitate of **1** was collected by filtration and rinsed several times with a cold 9:1
585 water:ethanol mixture. The resulting powder was then dried under vacuum for two days.
586 Yield: 220 mg, 80 %. ^{1}H NMR (300 MHz, $CDCl_3$) δ_H = 9.17 (1H, qd, J = 5.5 Hz), 8.18 (2H,
587 m, J = 1.3 Hz), 8.07 (2H, m, J = 1.6 Hz), 7.89 (1H, dd, J = 1.3 Hz), 7.56 (1H, m, J = 5.5 Hz),
588 5.03 (2H, dd, J = 12 Hz) ppm. ESI-MS analysis (positive mode) m/z = 518.9 [M-Br]$^+$. IR
589 (KBr pellet), $\nu_{C\equiv O}$: 2021 cm^{-1}, 1905 cm^{-1}, 1896 cm^{-1}. UV-Vis ($CHCl_3$, nm): 301, 386. Crystals
590 suitable for X-ray diffraction were obtained from slow evaporation of a deuterated
591 chloroform solution.

592 Complexes **2**-**6** were prepared according to the following general procedure. Under inert
593 conditions at RT, to a stirring solution of **1** (50 mg, 0.083 mmol) in 8 mL dichloromethane
594 the corresponding secondary amine (1 eq.) and N,N-diisopropylethylamine (DIPEA 1 eq.)
595 were added. The reaction mixture was then refluxed overnight under argon. After it had
596 cooled to RT, the reaction mixture was washed 3 times with bi-distilled water and then with
597 brine. The organic phase was separated, dried over $MgSO_4$, filtered and the solvent removed
598 under reduced pressure. The obtained powder was then dissolved in a minimum amount of
599 dichloromethane and 40 mL pentane were added before placing the flask in the fridge. After
600 a few days, a crystalline powder was filtered to yield the pure compounds. For compound **3**
601 sodium tert-butoxide was used instead of DIPEA.

602 ***fac*-[Re(CO)$_3$L$_2$Br] (L$_2$ = N-([2,2'-bipyridin]-6-ylmethyl)-N-ethylethanamine), 2.**
603 Yield: 23 mg, 47 %. ^{1}H NMR (300 MHz, $CDCl_3$) δH = 9.13 (1H, md, J = 7.8 Hz), 8.18 (2H,
604 d, J = 8.2 Hz), 8.03 (3H, m), 7.50 (1H, m), 4.18 (2H, dd, J = 25.7 Hz), 2.71 (4H, q, J = 7.1 Hz)
605 1.10 (6H, t, J = 7.1 Hz) ppm. ESI-MS analysis (positive mode) m/z = 512.2 [M-Br]$^+$. IR (KBr
606 pellet), $\nu_{C\equiv O}$: 2018 cm^{-1}, 1910 cm^{-1}, 1894 cm^{-1}. UV-Vis ($CHCl_3$, nm): 300, 385.

607 ***fac*-[Re(CO)$_3$L$_2$Br] (L$_2$ =**
608 **N-([2,2'-bipyridin]-6-ylmethyl)-N-isopropylpropan-2-amine), 3.** Yield: 15 mg, 30 %. ^{1}H
609 NMR (400 MHz, $CDCl_3$) δ_H = 9.14 (1H, d, J = 5.5 Hz), 8.27 (1H, d, J = 7.1 Hz), 8.17 (1H, d,
610 J = 8.2 Hz), 8.03 (2H, m), 7.97 (1H, m), 7.50 (1H, m), 4.27 (1H, d, J = 17.7 Hz), 4.15 (1H, d,
611 J = 17.8 Hz), 3.15 (2H, m), 1.09 (12H, d, J= 6.4 Hz) ppm. ESI-MS analysis (positive mode)
612 m/z =540.9 [M-Br]$^+$. IR (KBr pellet), $\nu_{C\equiv O}$: 2019 cm^{-1}, 1910 cm^{-1}, 1894 cm^{-1}. UV-Vis

($CHCl_3$, nm): 301, 388. Crystals suitable for X-ray diffraction were obtained by slow evaporation of deuterated chloroform.

***fac*-[Re(CO)$_3$L$_2$Br] (L$_2$ = N-([2,2'-bipyridin]-6-ylmethyl)-N-isobutyl-2-methylpropan-1-amine), 4.** Yield: 32 mg, 60 %. ^{1}H NMR (300 MHz, $CDCl_3$) δ_H = 9.12 (1H, d, J = 5.5 Hz), 8.2 (2H, m), 8.03 (3H, m), 7.50 (1H, m), 4.28 (1H, d, J = 16 Hz), 4.03 (1H, d, J =16 Hz), 2.32 (4H, m), 1.86 (2H, m), 0.94 (12H, m) ppm. ESI-MS analysis (positive mode) m/z = 568.0 $[M-Br]^+$. IR (KBr pellet), $\nu_{C\equiv O}$: 2019 cm^{-1}, 1911 cm^{-1}, 1896 cm^{-1}. UV-Vis ($CHCl_3$, nm): 300, 384. Crystals suitable for X-ray diffraction were obtained by vapor diffusion of pentane into a dichloromethane solution.

***fac*-[Re(CO)$_3$L$_2$Br] (L$_2$ = N^1-([2,2'-bipyridin]-6-ylmethyl)-N^1-(2-(diethylamino)ethyl)-N^2,N^2-diethylethane-1,2-diamine), 5.** Yield: 30 mg, 50 %. ^{1}H NMR (300 MHz, $CDCl_3$) δH = 9.07 (1H, d, J = 5.5 Hz), 8.23 (2H, dd, J = 18 Hz, J = 6.8 Hz), 8.03 (3H, m, J = 12.3 Hz), 7.47 (1H, m), 4.28 (2H, dd, J = 20.8 Hz), 2.71 (8H, m, J = 6.5 Hz), 2.54 (8H, q, J = 7.1 Hz), 0.99 (12H, t, J = 7.1 Hz) ppm. ESI-MS analysis (positive mode) m/z = 654.4 $[M-Br]^+$. IR (KBr pellet), $\nu_{C\equiv O}$: 2019 cm^{-1}, 1911 cm^{-1}, 1894 cm^{-1}. UV-Vis ($CHCl_3$, nm): 300, 379.

***fac*-[Re(CO)$_3$L$_2$Br] (L$_2$ = 1-([2,2'-bipyridin]-6-yl)-N,N-bis(pyridin-2-ylmethyl) methanamine), 6.** Yield: 36 mg, 60 %. ^{1}H NMR (300 MHz, $CDCl_3$) δ_H = 9.11 (1H, m), 8.59 (2H, m), 8.43 (1H, dd, J = 3.0 Hz), 8.15 (1H, d, J = 8.2 Hz), 7.99 (3H, m), 7.65 (2H, m), 7.49 (3H, m), 7.16 (2H, m), 4.45 (2H, bs), 4.04 (4H, bs) ppm. ESI-MS analysis (positive mode) m/z = 637.8 $[M-Br]^+$. IR (KBr pellet), $\nu_{C\equiv O}$: 2019 cm^{-1}, 1912 cm^{-1}, 1896 cm^{-1}. UV-Vis ($CHCl_3$, nm): 299, 385.

***fac*-[Re(CO)$_3$Br]L$_2$[Re(CO)$_3$] (L$_2$ = 1-([2,2'-bipyridin]-6-yl)-N,N-bis(pyridin-2-ylmethyl) methanamine), 7.** 165 mg of $[Re(CO)_3Br_3](Et_4N)_2$ (0.214 mmol) were dissolved in 5 mL water at room temperature. 0.5 eq. (36 mg, 0.098 mmol) of the ligand DPA-bpy in 5 mL ethanol were slowly added, and the mixture was then stirred overnight. After filtration, yellow crystals were obtained of the pure compound. Crystals suitable for X-ray diffraction were obtained by vapor diffusion of ether into a solution of the compound in dichloromethane. Yield: 42 mg, 40 %. ^{1}H NMR (300 MHz, CD_3OD) δ_H = 9.13 (1H, md, J = 5.55 Hz), 8.92 (1H, d, J = 13.6 Hz), 8.87 (1H, d, J = 13.6 Hz), 8.80 (1H, d, J = 1.1 Hz), 8.67 (1H, d, J = 8.2 Hz), 8.50 (1H, t, J = 7.9 Hz), 8.41 (1H, dd, J = 7.1 Hz), 8.30 (1H, td, J = 1.5 Hz), 7.92 (2H, m, J = 7.8 Hz), 7.73 (1H, m, J = 7.1 Hz), 7.55 (1H, d, J = 13.8 Hz), 7.5 (1H, d, J = 7.9 Hz), 7.39 (2H, m), 5.87 (2H, s), 5.63 (1H, d, J =

17.2 Hz), 5.06 (1H, d, J = 15.6 Hz), 4.77 (1H, d, J = 15.7 Hz), 4.62 (1H, d, J = 17.2 Hz) ppm. ESI-MS analysis (positive mode) m/z = 987.8 $[M]^+$. IR (KBr pellet), $\nu_{C\equiv O}$: 2028 cm^{-1}, 1943 cm^{-1}, 1921 cm^{-1}, 1889 cm^{-1}. UV-Vis ($CHCl_3$, nm): 299, 385.

***fac*-[Re(CO)$_3$L$_2$](NO$_3$) (L$_2$ = 1-([2,2'-bipyridin]-6-yl)-N,N-bis(pyridin-2-ylmethyl) methanamine), 8.** 385 mg (0.500 mmol) of $[Re(CO)_3Br_3](Et_4N)_2$ were dissolved in 10 mL H_2O to which a 10 mL aqueous solution of silver nitrate (255 mg) was added. The mixture was refluxed for 2.5h and the AgBr precipitate filtered over paper. The filtrate was added to a solution of the ligand DPA-bpy (184 mg, 0.501 mmol, in 1:1 H_2O:MeOH) and heated to 80°C overnight. After removal of the methanol by rotary evaporation, 137 mg of yellowish crystals formed over 2 days in the remaining aqueous mother liquor and were filtered to yield the pure compound. These crystals were found suitable for X-ray diffraction measurements. Yield: 137 mg, 40 %. ^{1}H NMR (300 MHz, CD_3OD) δ_H = 8.87 (2H, d, J = 5.5 Hz), 8.68 (1H, dm, J = 2.1 Hz), 8.47 (1H, d, J = 0.9 Hz), 8.39 (1H, d, J = 1.0 Hz), 8.10 (1H, t, J = 7.8 Hz), 7.92 (3H, m, J = 1.5 Hz), 7.78 (1H, d, J = 0.9 Hz), 7.51 (2H, d, J = 7.9 Hz), 7.46 (1H, m, J = 2.7 Hz), 7.36 (2H, m, J = 13.2 Hz), 5.47 (2H, d, J = 16.5 Hz), 5.12 (2H, s), 4.78 (2H, d, J = 16.5 Hz) ppm. ESI-MS analysis (positive mode) m/z = 638.0 $[M]^+$. IR (KBr pellet), $\nu_{C\equiv O}$: 2025 cm^{-1}, 1925 cm^{-1}, 1898 cm^{-1}. UV-Vis ($CHCl_3$, nm): 283, 332 (shoulder).

4.4 Interaction with hen egg white lysozyme (HEWL).

Sock solutions of HEWL and of **1** or **4** were mixed to a final concentration of 100 μM HEWL and 1 mM **1** or **4** (*ca.* 10 eq., 2mL water/DMSO, ϕDMSO = 0.6, below the denaturation conditions of HEWL) [144]. The reaction mixtures were gently vortexed 5 s, and then incubated at 37 ºC for 2 days. The mixtures were purified in portions by HPLC. In order to avoid possible denaturation of the enzyme, the fractions were collected in flask containing distilled water, always maintaining the ϕMeOH fraction below enzymatic denaturation conditions (ϕMeOH = 0.3 at pH 1.9) [145]. The different fractions were directly analyzed by ESI-MS (positive mode).

4.5 Nucleobase and Amino Acid Binding.

The interaction of complexes **1** and **4** with DNA nucleobase models guanine (G) and adenine (A) was investigated by NMR spectroscopy in a DMSO-d6 solution (0.5 mM **1** or **4**, + 2 eq. DNA base). No binding of the complexes to either G or A was observed after 48 h incubation at 37 °C. The interaction of the same complexes with Fmoc-protected Lys-OH, Asn-OH and Gln-OH was probed by ESI-MS (positive mode). Solutions containing

combinations of **1** and **4** (100 µM) with the aa (2 eq.) were prepared in 0.5 mL water/DMSO, ϕDMSO = 0.7, pH = 7.3 and incubated for 48 h at 37 °C before analysis.

4.6 Cytotoxicity evaluation.

Antiproliferative activity was tested in a panel of tumor cells including A549 (ling adenocarcinoma cells), HCT-116 (colorectal carcinoma cells), Mia PaCa-2 (pancreatic carcinom acells) and HeLa, (cervix carcinoma cells), as well as on normal human lung fibroblasts (MRC-5), all from ATCC collection. Compounds were freshly dissolved in DMSO and used for the bioactivity assessments. Cytotoxicity in terms of antiproliferative effects was tested by the standard 3-(4,5-dimethylthiazol-2-yl)-2,5-diphenyltetrazolium bromide (MTT) assay [146]. The assay was carried out after 48 h of cell monolayer incubation in the RPMI-1640 medium supplemented with 100 µg mL-1 streptomycin, 100 U mL-1 penicillin and 10% (v/v) fetal bovine serum (FBS) (all from Sigma, Munich, Germany), containing different concentrations of the compounds in four replicates, two times. Cells were grown in humidified atmosphere of 95% air and 5% CO_2 at 37 °C. The extent of MTT reduction was measured spectrophotometrically at 540 nm using Tekan Infinite 200 Pro multiplate reader (Tecan Group Ltd., Männedorf, Switzerland). Cytotoxicity was expressed as the concentration of the compound inhibiting cell growth by 50% (IC_{50}) in comparison to the untreated control.

4.7 Cellular uptake and Fluorescent microscopy.

Approximately 2×10^5 HCT-116 cells were grown in RPMI-1640 medium on glass cover slips in 6-well microtiter plates, up to reaching the confluency. To address whether the cellular uptake of the complexes was mediated by energy-dependent process, monolayer of HCT-116 cells was treated with **1** and **4** (5 µM) and incubated at 4 °C or 37 °C for 30 min in RPMI medium. To address intracellular localization of **1** and **4**, HCT-116 cells monolayer was incubated for 30 min at 37 °C and 5% CO_2 in RPMI medium with LysoTracker® Deep Red (25 nM, Thermofisher Scientific) and/or **1** and **4** (5 µM). Cells were subsequently fixed with 4% formaldehyde for 20 min at room temperature, washed twice with PBS and analysed or stained with DAPI [4,6-diamidino-2-phenylindole, dihydrochloride] (14.3 µM, Thermofisher Scientific) and later analysed. Stained cells were observed under a fluorescence microscope (Olympus BX51, Applied Imaging Corp., San Jose, CA, United States) under × 100 magnification.

4.8 DNA interactions.

DNA interaction assay using gel electrophoresis was conducted according to the previously published procedure using commercial lambda bacteriophage DNA (100 ng, Thermo Scientific™) [147]. DNA solution of the final concentration 20 ng/μL was incubated with 50, 100, 250 and 500 μM of **1** and **4** in 10 mM Tris-Cl, (pH 8.5) in 15 μL reaction volume. Control contained an appropriate volume of DMSO. After 2 h incubation at 37 °C, samples were mixed with loading dye and run on 0.8% agarose gel with ethidium bromide (EtBr) against a 1 kb DNA Ladder Plus (NIPPON Genetics Europe) at 60 V for 2 h. Gels were visualized and analysed using the Gel Doc EZ system (Bio-Rad, Life Sciences, Hercules, USA), equipped with the Image Lab™ Software.

4.9 In vivo toxicity assessment.

Toxicity evaluation of Re(I)-tricarbonyl complexes was carried in the zebrafish (*Danio rerio*) model according to the general rules of the OECD Guidelines for the Testing of Chemicals (OECD, 2013, Test No. 236) [148]. All experiments involving zebrafish were performed in compliance with the European directive 2010/63/EU and the ethical guidelines of the Guide for Care and Use of Laboratory Animals of the Institute of Molecular Genetics and Genetic Engineering, University of Belgrade. Wild type (AB) zebrafish were kindly provided by dr Ana Cvejić (Wellcome Trust Sanger Institute, Cambridge, UK), raised to adult stage in a temperature- and light-controlled zebrafish facility at 28 °C and standard 14:10-hour light-dark photoperiod, and regularly fed with commercially dry flake food (TetraMin™ flakes; Tetra Melle, Germany) twice a day and Artemia nauplii once daily. Embryos were produced by pair-wise mating, collected and distributed into 24-well plates containing 10 embryos per well and 1 mL embryos water (0.2 g/L of Instant Ocean® Salt in distilled water) and raised at 28 °C. For assessing lethality and developmental toxicity, the embryos staged at 6 hours post fertilization (hpf) were exposed to different concentrations of the tested compounds, and inspected for apical endpoints (Table S1) every day by 120 hpf upon an inverted microscope (CKX41; Olympus, Tokyo, Japan). Dead embryos were counted and discarded every 24 h. DMSO (0.25%) was used as negative control. Experiments were performed three times using 30 embryos per concentration. At 120 hpf, embryos were inspected for heartbeat rate, anesthetized by addition of 0.1% (w/v) tricaine solution (Sigma-Aldrich, St. Louis, MO), photographed and killed by freezing at -20 °C for ≥ 24 h.

In addition to developmental toxicity, anticancer Re(I)tricarbonyl complexes with the best therapeutic profile, **1** and **4**, were selected and evaluated for myelotoxicity and hepatoxicity. Myelotoxicity (neutropenia and inflammation) was addressed in the transgenic *Tg*(*mpx*:GFP) zebrafish embryos, which express green fluorescent protein (GFP) in neutrophils [149], enabling thus direct visualization of the effect of applied treatments on the neutrophils occurrence. Embryos of *Tg*(*mpx*:GFP) zebrafish were kindly provided by Dr. Ana Cvejic (Wellcome Trust Sanger Institute, Cambridge, UK) and raised in our zebrafish facility to adult stage under previously described life conditions. At 6 hpf stage, embryos were exposed to various non-toxic concentrations of the selected complexes and incubated at 28 °C by 120 hpf. At 120 hpf, embryos were imaged for the neutrophils occurrence under a fluorescence microscope (Olympus BX51, Applied Imaging Corp., San Jose, CA, USA), and the neutrophils occurrence (fluorescence intensity) was determined using ImageJ programme (NIH public domain software; NIH is National Institutes of Health). The experiment was performed three times using 10 embryos per a concentration. Hepatotoxicity was determined using transgenic *Tg*(-2.*8fabp10a*:EGFP) zebrafish embryos with the fluorescently labelled liver [150]. Embryos were exposed to the non-toxic doses of the tested complexes at the 72 hpf (a stage when the liver is fully functional, vascularized and started metabolic transformation of absorbed compounds) and processed by fluorescent microscopy at 120 hpf. Experiment was performed two times using 10 embryos per concentration. The liver toxicity was evaluated in relation to the control group according to various hepatotoxicity endpoints such as the liver area index (the ration between liver area and embryonic lateral area x 100%) [151], the liver colour and the yolk retention [152]. In all mentioned toxicity assays, sunitinib malate (Suten, Pfizer, New York), doxorubicin (Actavis, S.C. Sindan-Pharma S.R.L., Romania) and cisplatin (Merck KGaA,Darmstadt, Germany) were used as the control, clinically approved drugs at the previously reported effective doses.

4.10 Anti-angiogenic activity evaluation.

The angiogenesis inhibitory activity of anticancer Re(I) tricarbonyl complexes with the best therapeutic profile was addressed in transgenic zebrafish *Tg*(*fli1*:EGFP) embryos with EGFP-labelled endothelial cells, as previously described [83]. Briefly, zebrafish embryos at 6 hpf stage were exposed to the range of non-toxic concentrations of the selected complexes, and incubated at 28 °C by 48 hpf. At 48 hpf, the treated embryos were anesthetized with 0.02% tricaine, imaged under a fluorescence microscope (Olympus BX51, Applied Imaging Corp., San Jose, CA, USA) and analysed for the development of intersegmental blood vessels (ISVs), subintestinal vessels (SIVs) and dorsal longitudinal anastomotic vessels

(DLAVs). Sunitinib malate was used as a positive control. The experiments were performed three times using 10 embryos per concentration. ISV and SIV lengths were measured using Image J programme and expressed as mean value with standard deviation. Inhibitory effect of applied treatments was determined in relation to the control group, arbitrarily set to 100%.

4.11 Anticancer activity evaluation in human CRC-zebrafish xenografts

The human colorectal HCT-116 cell line was cultured in RPMI-1640 supplemented with 10 % FBS, 100 µg/mL streptomycin and 100 UmL^{-1} penicillin, and grown as a monolayer in humidified atmosphere of 95% air and 5% CO_2 at 37 °C. Prior to microinjection, the cells were washed once with PBS and trypsinized (0.25% trypsin/0.53 mM EDTA) to obtain a single cell suspension. After centrifugation at 1200 rpm for 5 min, the cells were resuspended in serum-free RPMI medium and labelled with 2 µM CellTracker™ RedCMTPX (Thermofisher Scientific) according to the manufacturer's instructions.

4.12 Zebrafish xenografts injection and Treatment.

The zebrafish xenografts with human HCT-116 cells were established according to the previously described procedure [153]. Before the microinjections, *Tg*(*fli1*:EGFP) embryos were kept at 28 °C and manually dechorionated few hours before the injection. At 48 hpf, 5 nL of cells suspension containing 150 labelled cells was microinjected into the yolk of anesthetized embryos by a pneumatic picopump (PV820, World Precision Instruments, USA). Exact number of cells was confirmed by dispensing the injected volume onto a microscope slide and by visual counting. After injection, embryos were incubated to recover for at least one hour at 28 °C, dead embryos were removed, and alive embryos were transferred into 24-well plates containing 1 mL of embryo water and 10 embryos per well. The injected xenografts were treated with different doses of complex **1** and **4** (1/2, 1/4 and 1/8 of IC_{50} values), and maintained at 33 °C by 120 hpf. DMSO (0.25%) was used as a negative control and cisplatin as a positive control at the maximum tolerated concentration (34 µM) [105]. The survival and development of the xenografted embryos was recorded every day until the end of experiment. At 3 days post injection (dpi), anesthetized xenografts were processed by fluorescent microscopy. We quantified tumor size, the number of xenografts with disseminated cells in caudal region, and the number of disseminated cells per embryo. The tumour size was determined by the fluorescent images using ImageJ programme. The experiment was repeated two times.

4.13 Statistical analysis.

The experimental results were expressed as mean values ± SD. The differences in anti-angiogenic phenotypes between the untreated and treated groups were determined according to χ^2 test. In other tests, the differences between the untreated and treated groups, as well as between the treatments were evaluated using the one-way ANOVA followed by a comparison of the means by Bonferroni test (P = 0.05). All analyses were performed using SPSS 20 (SPSS Inc., Chicago, IL) software package.

Supplementary Materials: The following are available online at www.mdpi.com/xxx/s1, Figures S1-S8: ^{1}H NMR spectra of complexes **1**-**8** respectively, Figures S9: HPLC trace of **1**, Figures S10: HPLC trace of **4**, Figures S11: UV-Vis spectra of **1**-**8**, Figures S12: Fluorescence emission spectra of complexes **1**-**8**, Figure S13: Anticancer activity of cisplatin in human HCT-116 cells zebrafish xenografts, Figure S14: Electrospray ionization mass spectrum of HEWL mixed with **1**, Figures S15-S16: Electrospray ionization mass spectra of Fmoc-Lys-OH mixed with **1** and **4** respectively, Figure S17. Gel electrophoresis of *in vitro* interaction of complexes **1** and **4** with lambda bacteriophage DNA, Figure S18. ^{1}H NMR spectra of (bottom to top) complex **1** alone, with 2 eq. of guanine and adenine incubated in DMSO at 37 °C for two days, Figure S19. ^{1}H NMR spectra of (bottom to top) complex **4** alone, with 2 eq. of guanine and adenine incubated in DMSO at 37 °C for two days, Table S1: Lethal and teratogenic effects observed in zebrafish (*Danio rerio*) embryos at different hours post fertilization (hpf).

Author Contributions: F.Z. designed and coordinated the overall experimental program with the help of J.N.R. J.D. and N.V. synthesized and characterized the complexes and studied their chemical reactions (J.D.). S.V. and J.N.R. designed and carried out the *in vitro* studies. A.P. designed and carried out the *in vivo* studies. A.C. carried out the X-ray crystallography. J.D., A.P. and F.Z. wrote the manuscript, and all authors contributed to the final version.

Funding: Financial support from the Swiss National Science Foundation (Grant# PP00P2_170589), the University of Fribourg and the Institute of Molecular Genetics and Genetic Engineering from the University of Belgrade (Ministry of Education, Science and Technological Development of the Republic of Serbia, Project No.173048 (to A.P., S.V. and J.N.R.)) are gratefully acknowledged.

Conflicts of Interest: The authors declare that they have no known competing financial interests or personal relationships that could have appeared to influence the work reported in this paper.

Abbreviations Used.

bpy-DPA, 1-([2,2'-bipyridin]-6-yl)-N,N-bis(pyridin-2-ylmethyl)methanamine; CRC, colorectal carcinomas; CCDC, Cambridge crystallographic data centre; DAPI, 4′,6-diamidino-2-phenylindole; DLAVs, dorsal lateral vessels; DMSO, dimethyl sulfoxide; EGFP, enhanced green fluorescent protein; EC_{50}, effective concentration resulting in toxic response of 50% of embryos; HEWL, hen egg white lysozyme; hpf, hours post-fertilization; $ED_{50\text{-}HCT116}$, effective drug concentration reducing tumour mass by 50% in relation to that in untreated xenografts; Fmoc, fluorenylmethyloxycarbonyl protecting group; IC_{50ang}, the concentration upon which 50% of embryos displayed anti-angiogenic phenotype; ISVs, intersegmental vessels; LC_{50}, concentration of the compound in feed (or water in case of fish) that is lethal for 50% of exposed population; Tw, therapeutic window.

References

[1] W.I.A.F.R.O. Cancer, Latest global cancer data, in, 2018.

[2] N. Keum, E. Giovannucci, Global burden of colorectal cancer: emerging trends, risk factors and prevention strategies, Nat. Rev. Gastroenterol. Hepatol., 16 (2019) 713-732.

[3] A. Lopez, K. Harada, M. Vasilakopoulou, N. Shanbhag, J.A. Ajani, Targeting Angiogenesis in Colorectal Carcinoma, Drugs, 79 (2019) 63-74.

[4] J. Delasoie, J. Rossier, L. Haeni, B. Rothen-Rutishauser, F. Zobi, Slow-targeted release of a ruthenium anticancer agent from vitamin B-12 functionalized marine diatom microalgae, Dalton Trans., 47 (2018) 17221-17232.

[5] J. Delasoie, F. Zobi, Natural Diatom Biosilica as Microshuttles in Drug Delivery Systems, Pharmaceutics, 11 (2019) 537.

[6] A. Leonidova, V. Pierroz, R. Rubbiani, J. Heier, S. Ferrari, G. Gasser, Towards cancer cell-specific phototoxic organometallic rhenium(I) complexes, Dalton Trans., 43 (2014) 4287-4294.

[7] F.L. Thorp-Greenwood, R.G. Balasingham, M.P. Coogan, Organometallic complexes of transition metals in luminescent cell imaging applications, J. Organomet. Chem. , 714 (2012) 12-21.

[8] V. Fernandez-Moreira, F.L. Thorp-Greenwood, M.P. Coogan, Application of d6 transition metal complexes in fluorescence cell imaging, Chem. Commun., 46 (2010) 186-202.

[9] K.K.-W. Lo, M.-W. Louie, K.Y. Zhang, Design of luminescent iridium(III) and rhenium(I) polypyridine complexes as *in vitro* and *in vivo* ion, molecular and biological probes, Coord. Chem. Rev., 254 (2010) 2603-2622.

[10] V. Fernández-Moreira, F.L. Thorp-Greenwood, A.J. Amoroso, J. Cable, J.B. Court, V. Gray, A.J. Hayes, R.L. Jenkins, B.M. Kariuki, D. Lloyd, C.O. Millet, C.F. Williams, M.P. Coogan, Uptake and localisation of rhenium fac-tricarbonyl polypyridyls in fluorescent cell imaging experiments, Org. Biomol. Chem., 8 (2010) 3888-3901.

[11] A. Leonidova, G. Gasser, Underestimated Potential of Organometallic Rhenium Complexes as Anticancer Agents, ACS Chem. Biol., 9 (2014) 2180-2193.

[12] N.A. Illan-Cabeza, A.R. Garcia-Garcia, M.N. Moreno-Carretero, J.M. Martinez-Martos, M.J. Ramirez-Exposito, Synthesis, characterization and antiproliferative behavior of tricarbonyl complexes of rhenium(I) with some 6-amino-5-nitrosouracil derivatives: Crystal structure of fac-[ReCl(CO)(3)(DANU-N-5,O-4)] (DANU=6-amino-1, 3-dimethyl-5-nitro souracil), J. Inorg. Biochem., 99 (2005) 1637-1645.

[13] J.M. Ho, W.Y. Lee, K.J.T. Koh, P.P.F. Lee, Y.K. Yan, Rhenium(I) tricarbonyl complexes of salicylaldehyde semicarbazones: Synthesis, crystal structures and cytotoxicity, J. Inorg. Biochem., 119 (2013) 10-20.

[14] C.-C. Pagoni, V.-S. Xylouri, G.C. Kaiafas, M. Lazou, G. Bompola, E. Tsoukas, L.C. Papadopoulou, G. Psomas, D. Papagiannopoulou, Organometallic rhenium tricarbonyl–enrofloxacin and –levofloxacin complexes: synthesis, albumin-binding, DNA-interaction and cell viability studies, J. Biol. Inorg. Chem., 24 (2019) 609-619.

[15] J.Y. Zhang, J.J. Vittal, W. Henderson, J.R. Wheaton, I.H. Hall, T.S.A. Hor, Y.K. Yan, Tricarbonylrhenium(I) complexes of phosphine-derivatized amines, amino acids and a model peptide: structures, solution behavior and cytotoxicity, J. Organomet. Chem., 650 (2002) 123-132.

[16] A. Kermagoret, G. Morgant, J. d'Angelo, A. Tomas, P. Roussel, G. Bastian, P. Collery, D. Desmaele, Synthesis, structural characterization and biological activity against several human tumor cell lines of four rhenium(I) diseleno-ethers complexes: Re(CO)(3)Cl(PhSe(CH2)(2)SePh), Re(CO)(3)Cl(PhSe(CH2)(3)SePh), Re(CO)(3)Cl(HO2C-CH2Se(CH2)(2)SeCH2-CO2H) and Re(CO)(3)Cl(HO2C-CH2Se(CH2)(3)SeCH2-CO2H), Polyhedron, 30 (2011) 347-353.

[17] P. Collery, F. Santoni, J. Ciccolini, T.N. Tran, A. Mohsen, D. Desmaele, Dose Effect of Rhenium (I)-diselenoether as Anticancer Drug in Resistant Breast Tumor-bearing Mice After Repeated Administrations, Anticancer Res., 36 (2016) 6051-6057.

[18] P. Collery, A. Mohsen, A. Kermagoret, S. Corre, G. Bastian, A. Tomas, M. Wei, F. Santoni, N. Guerra, D. Desmaele, J. d'Angelo, Antitumor activity of a rhenium (I)-diselenoether complex in experimental models of human breast cancer, Invest. New Drugs, 33 (2015) 848-860.

[19] P. Collery, G. Bastian, F. Santoni, A. Mohsen, M. Wei, T. Collery, A. Tomas, D. Desmaele, J. D'Angelo, Uptake and efflux of rhenium in cells exposed to rhenium diseleno-ether and tissue distribution of rhenium and selenium after rhenium diseleno-ether treatment in mice, Anticancer Res., 34 (2014) 1679-1689.

[20] P. Collery, V. Veena, A. Harikrishnan, D. Desmaele, The rhenium(I)-diselenoether anticancer drug targets ROS, TGF-β1, VEGF-A, and IGF-1 in an *in vitro* experimental model of triple-negative breast cancers, Invest. New Drugs, 37 (2019) 973-983.

[21] N. Viola-Villegas, A.E. Rabideau, J. Cesnavicious, J. Zubieta, R.P. Doyle, Targeting the folate receptor (FR): Imaging and cytotoxicity of Re-I conjugates in FR-overexpressing cancer cells, Chemmedchem, 3 (2008) 1387-1394.

[22] N. Viola-Villegas, A.E. Rabideau, M. Bartholoma, J. Zubieta, R.P. Doyle, Targeting the Cubilin Receptor through the Vitamin B-12 Uptake Pathway: Cytotoxicity and Mechanistic Insight through Fluorescent Re(I) Delivery, J. Med. Chem., 52 (2009) 5253-5261.

[23] M.D. Bartholoma, A.R. Vortherms, S. Hillier, B. Ploier, J. Joyal, J. Babich, R.P. Doyle, J. Zubieta, Synthesis, Cytotoxicity, and Insight into the Mode of Action of Re(CO)(3) Thymidine Complexes, Chemmedchem, 5 (2010) 1513-1529.

[24] M.D. Bartholoma, A.R. Vortherms, S. Hillier, J. Joyal, J. Babich, R.P. Doyle, J. Zubieta, Synthesis, cytotoxicity and cellular uptake studies of N3 functionalized Re(CO)(3) thymidine complexes, Dalton Trans., 40 (2011) 6216-6225.

[25] I. Kitanovic, S.Z. Can, H. Alborzinia, A. Kitanovic, V. Pierroz, A. Leonidova, A. Pinto, B. Spingler, S. Ferrari, R. Molteni, A. Steffen, N. Metzler-Nolte, S. Wolfl, G. Gasser, A Deadly Organometallic Luminescent Probe: Anticancer Activity of a ReI Bisquinoline Complex, Chem. Eur. J., 20 (2014) 2496-2507.
[26] A.J. North, D.J. Hayne, C. Schieber, K. Price, A.R. White, P.J. Crouch, A. Rigopoulos, G.J. O'Keefe, H. Tochon-Danguy, A.M. Scott, J.M. White, U. Ackermann, P.S. Donnelly, Toward hypoxia-selective rhenium and technetium tricarbonyl complexes, Inorg. Chem., 54 (2015) 9594-9610.
[27] Y.K. Yan, S.E. Cho, K.A. Shaffer, J.E. Rowell, B.J. Barnes, I.H. Hall, Cytotoxicity of rhenium(I) alkoxo and hydroxo carbonyl complexes in murine and human tumor cells, Pharmazie, 55 (2000) 307-313.
[28] W.W. Wang, Y.K. Yan, T.S.A. Hor, J.J. Vittal, J.R. Wheaton, I.H. Hall, Synthesis, X-ray structures, and cytotoxicity of rhenium(I) carbonyl 2-(dimethylamino)ethoxide complexes, Polyhedron, 21 (2002) 1991-1999.
[29] V. Scarcia, A. Furlani, B. Longato, B. Corain, G. Pilloni, Heteropolymetallic Complexes of 1,1'-Bis(Diphenylphosphino)Ferrocene (Dppf) .4. Solvolytic Behavior and Cytostatic Properties Towards the Kb Cell-Line of Dppf and 1,2-Bis(Diphenylphosphino)Ethane Cis-Complexes of Pt(Ii) and Pd(Ii), Inorg. Chim. Acta Bioinorg. Chem., 153 (1988) 67-70.
[30] A. Kastl, S. Dieckmann, K. Wahler, T. Volker, L. Kastl, A.L. Merkel, A. Vultur, B. Shannan, K. Harms, M. Ocker, W.J. Parak, M. Herlyn, E. Meggers, Rhenium Complexes with Visible-Light-Induced Anticancer Activity, Chemmedchem, 8 (2013) 924-927.
[31] T. Gianferrara, C. Spagnul, R. Alberto, G. Gasser, S. Ferrari, V. Pierroz, A. Bergamo, E. Alessio, Towards Matched Pairs of Porphyrin-ReI/99mTcI Conjugates that Combine Photodynamic Activity with Fluorescence and Radio Imaging, Chemmedchem, 9 (2014) 1231-1237.
[32] A. Leonidova, V. Pierroz, R. Rubbiani, Y.J. Lan, A.G. Schmitz, A. Kaech, R.K.O. Sigel, S. Ferrari, G. Gasser, Photo-induced uncaging of a specific Re(I) organometallic complex in living cells, Chem. Sci., 5 (2014) 4044-4056.
[33] A. Leonidova, V. Pierroz, R. Rubbiani, J. Heier, S. Ferrari, G. Gasser, Towards cancer cell-specific phototoxic organometallic rhenium(I) complexes, Dalton Trans., 43 (2014) 4287-4294.
[34] S.C. Marker, S.N. MacMillan, W.R. Zipfel, Z. Li, P.C. Ford, J.J. Wilson, Photoactivated *in vitro* Anticancer Activity of Rhenium(I) Tricarbonyl Complexes Bearing Water-Soluble Phosphines, Inorg. Chem., 57 (2018) 1311-1331.
[35] I. Chakraborty, J. Jimenez, W.M.C. Sameera, M. Kato, P.K. Mascharak, Luminescent Re(I) Carbonyl Complexes as Trackable PhotoCORMs for CO delivery to Cellular Targets, Inorg. Chem., 56 (2017) 2863-2873.
[36] I. Chakraborty, J. Jimenez, P.K. Mascharak, CO-Induced apoptotic death of colorectal cancer cells by a luminescent photoCORM grafted on biocompatible carboxymethyl chitosan, Chem. Commun., 53 (2017) 5519-5522.
[37] I. Chakraborty, S.J. Carrington, G. Roseman, P.K. Mascharak, Synthesis, Structures, and CO Release Capacity of a Family of Water-Soluble PhotoCORMs: Assessment of the Biocompatibility and Their Phototoxicity toward Human Breast Cancer Cells, Inorg. Chem., 56 (2017) 1534-1545.
[38] I. Chakraborty, S.J. Carrington, P.K. Mascharak, Photodelivery of CO by Designed PhotoCORMs: Correlation between Absorption in the Visible Region and Metal-CO Bond Labilization in Carbonyl Complexes, Chemmedchem, 9 (2014) 1266-1274.
[39] A.E. Pierri, A. Pallaoro, G. Wu, P.C. Ford, A Luminescent and Biocompatible PhotoCORM, J. Am. Chem. Soc. , 134 (2012) 18197-18200.
[40] K.K.W. Lo, K.Y. Zhang, S.P.Y. Li, Recent Exploitation of Luminescent Rhenium(I) Tricarbonyl Polypyridine Complexes as Biomolecular and Cellular Probes, Eur. J. Inorg. Chem., (2011) 3551-3568.

[41] S. Hostachy, C. Policar, N. Delsuc, Re(I) carbonyl complexes: Multimodal platforms for inorganic chemical biology, Coord. Chem. Rev., 351 (2017) 172-188.
[42] P. Collery, D. Desmaele, V. Vijaykumar, Design of Rhenium Compounds in Targeted Anticancer Therapeutics, Curr. Pharm. Des., 25 (2019) 1-17.
[43] E.B. Bauer, A.A. Haase, R.M. Reich, D.C. Crans, F.E. Kühn, Organometallic and coordination rhenium compounds and their potential in cancer therapy, Coord. Chem. Rev., 393 (2019) 79-117.
[44] C.C. Konkankit, S.C. Marker, K.M. Knopf, J.J. Wilson, Anticancer activity of complexes of the third row transition metals, rhenium, osmium, and iridium, Dalton Trans., 47 (2018) 9934-9974.
[45] A.J. Amoroso, M.P. Coogan, J.E. Dunne, V. Fernandez-Moreira, J.B. Hess, A.J. Hayes, D. Lloyd, C. Millet, S.J.A. Pope, C. Williams, Rhenium fac tricarbonyl bisimine complexes: biologically useful fluorochromes for cell imaging applications, Chem. Commun., (2007) 3066-3068.
[46] M.W. Louie, M.H.C. Lam, K.K.W. Lo, Luminescent Polypyridinerhenium(I) Bis-Biotin Complexes as Crosslinkers for Avidin, Eur. J. Inorg. Chem., (2009) 4265-4273.
[47] M.W. Louie, H.W. Liu, M.H.C. Lam, T.C. Lau, K.K.W. Lo, Novel Luminescent Tricarbonylrhenium(I) Polypyridine Tyramine-Derived Dipicolylamine Complexes as Sensors for Zinc(II) and Cadmium(II) Ions, Organometallics, 28 (2009) 4297-4307.
[48] A. Leonidova, V. Pierroz, L.A. Adams, N. Barlow, S. Ferrari, B. Graham, G. Gasser, Enhanced Cytotoxicity through Conjugation of a "Clickable" Luminescent Re(I) Complex to a Cell-Penetrating Lipopeptide, ACS Med. Chem. Lett., 5 (2014) 809-814.
[49] R.R. Ye, C.P. Tan, M.H. Chen, L. Hao, L.N. Ji, Z.W. Mao, Mono- and Dinuclear Phosphorescent Rhenium(I) Complexes: Impact of Subcellular Localization on Anticancer Mechanisms, Chem. Eur. J., 22 (2016) 7800-7809.
[50] S. Clede, F. Lambert, R. Saint-Fort, M.A. Plamont, H. Bertrand, A. Vessieres, C. Policar, Influence of the Side-Chain Length on the Cellular Uptake and the Cytotoxicity of Rhenium Triscarbonyl Derivatives: A Bimodal Infrared and Luminescence Quantitative Study, Chem. Eur. J., 20 (2014) 8714-8722.
[51] A.W.T. Choi, M.W. Louie, S.P.Y. Li, H.W. Liu, B.T.N. Chan, T.C.Y. Lam, A.C.C. Lin, S.H. Cheng, K.K.W. Lo, Emissive Behavior, Cytotoxic Activity, Cellular Uptake, and PEGylation Properties of New Luminescent Rhenium(I) Polypyridine Poly(ethylene glycol) Complexes, Inorg. Chem., 51 (2012) 13289-13302.
[52] B. Radaram, J.A. Ivie, W.M. Singh, R.M. Grudzien, J.H. Reibenspies, C.E. Webster, X. Zhao, Water Oxidation by Mononuclear Ruthenium Complexes with TPA-Based Ligands, Inorg. Chem., 50 (2011) 10564-10571.
[53] J.A. Platts, S.P. Oldfield, M.M. Reif, A. Palmucci, E. Gabano, D. Osella, The RP-HPLC measurement and QSPR analysis of logP(o/w) values of several Pt(II) complexes, J. Inorg. Biochem., 100 (2006) 1199-1207.
[54] A. Leo, C. Hansch, D. Elkins, Partition Coefficients and Their Uses, Chem. Rev., 71 (1971) 525-616.
[55] I.V. Tetko, P. Bruneau, Application of ALOGPS to predict 1-octanol/water distribution coefficients, logP, and logD, of AstraZeneca in-house database, J. Pharm. Sci., 93 (2004) 3103-3110.
[56] I.V. Tetko, V.Y. Tanchuk, Application of associative neural networks for prediction of lipophilicity in ALOGPS 2.1 program, J. Chem. Inf. Comput. Sci., 42 (2002) 1136-1145.
[57] K.M. Knopf, B.L. Murphy, S.N. MacMillan, J.M. Baskin, M.P. Barr, E. Boros, J.J. Wilson, *In vitro* Anticancer Activity and *in vivo* Biodistribution of Rhenium(I) Tricarbonyl Aqua Complexes, J. Am. Chem. Soc., 139 (2017) 14302-14314.
[58] S. Imstepf, V. Pierroz, R. Rubbiani, M. Felber, T. Fox, G. Gasser, R. Alberto, Organometallic Rhenium Complexes Divert Doxorubicin to the Mitochondria, Angew. Chem., Int. Ed., 55 (2016) 2792-2795.

[59] M.W. Louie, A.W.T. Choi, H.W. Liu, B.T.N. Chan, K.K.W. Lo, Synthesis, Emission Characteristics, Cellular Studies, and Bioconjugation Properties of Luminescent Rhenium(I) Polypyridine Complexes with a Fluorous Pendant, Organometallics, 31 (2012) 5844-5855.

[60] K.K.W. Lo, M.W. Louie, K.S. Sze, J.S.Y. Lau, Rhenium(I) polypyridine biotin isothiocyanate complexes as the first luminescent biotinylation reagents: Synthesis, photophysical properties, biological labeling, cytotoxicity, and imaging studies, Inorg. Chem., 47 (2008) 602-611.

[61] J. Skiba, A. Kowalczyk, P. Stączek, T. Bernaś, D. Trzybiński, K. Woźniak, U. Schatzschneider, R. Czerwieniec, K. Kowalski, Luminescent fac-[Re(CO)3(phen)] carboxylato complexes with non-steroidal anti-inflammatory drugs: synthesis and mechanistic insights into the *in vitro* anticancer activity of fac-[Re(CO)3(phen)(aspirin)], New J. Chem., 43 (2019) 573-583.

[62] C.C. Konkankit, A.P. King, K.M. Knopf, T.L. Southard, J.J. Wilson, *In vivo* Anticancer Activity of a Rhenium(I) Tricarbonyl Complex, ACS Med. Chem. Lett., 10 (2019) 822-827.

[63] C.C. Konkankit, B.A. Vaughn, S.N. MacMillan, E. Boros, J.J. Wilson, Combinatorial Synthesis to Identify a Potent, Necrosis-Inducing Rhenium Anticancer Agent, Inorg. Chem., 58 (2019) 3895-3909.

[64] C. Parson, V. Smith, C. Krauss, H.N. Banerjee, C. Reilly, J.A. Krause, J.M. Wachira, D. Giri, A. Winstead, S.K. Mandal, Anticancer Properties of Novel Rhenium Pentylcarbanato Compounds against MDA-MB-468(HTB-132) Triple Node Negative Human Breast Cancer Cell Lines, Br. J. Pharm. Res., 4 (2015) 362-367.

[65] I. Picón-Ferrer, F. Hueso-Ureña, N.A. Illán-Cabeza, S.B. Jiménez-Pulido, J.M. Martínez-Martos, M.J. Ramírez-Expósito, M.N. Moreno-Carretero, Chloro-fac-tricarbonylrhenium(I) complexes of asymmetric azines derived from 6-acetyl-1,3,7-trimethylpteridine-2,4(1H,3H)-dione with hydrazine and aromatic aldehydes: Preparation, structural characterization and biological activity against several human tumor cell lines, J. Inorg. Biochem., 103 (2009) 94-100.

[66] I. Kitanovic, S. Can, H. Alborzinia, A. Kitanovic, V. Pierroz, A. Leonidova, A. Pinto, B. Spingler, S. Ferrari, R. Molteni, A. Steffen, N. Metzler-Nolte, S. Wölfl, G. Gasser, A Deadly Organometallic Luminescent Probe: Anticancer Activity of a ReI Bisquinoline Complex, Chem. Eur. J., 20 (2014) 2496-2507.

[67] J. Yang, J.X. Zhao, Q. Cao, L. Hao, D.X. Zhou, Z.J. Gan, L.N. Ji, Z.W. Mao, Simultaneously Inducing and Tracking Cancer Cell Metabolism Repression by Mitochondria-Immobilized Rhenium(I) Complex, ACS Appl. Mater. Interfaces, 9 (2017) 13900-13912.

[68] L. He, Z.-Y. Pan, W.-W. Qin, Y. Li, C.-P. Tan, Z.-W. Mao, Impairment of the autophagy-related lysosomal degradation pathway by an anticancer rhenium(i) complex, Dalton Trans., 48 (2019) 4398-4404.

[69] M.K. Mbagu, D.N. Kebulu, A. Winstead, S.K. Pramanik, H.N. Banerjee, M.O. Iwunze, J.M. Wachira, G.E. Greco, G.K. Haynes, A. Sehmer, F.H. Sarkar, D.M. Ho, R.D. Pike, S.K. Mandal, Fac-tricarbonyl(pentylcarbonato)(alpha-diimine)rhenium complexes: One-pot synthesis, characterization, fluorescence studies, and cytotoxic activity against human MDA-MB-231 breast, CCl-227 colon and BxPC-3 pancreatic carcinoma cell lines, Inorg. Chem. Commun., 21 (2012) 35-38.

[70] M. Munoz-Osses, F. Godoy, A. Fierro, A. Gomez, N. Metzler-Nolte, New organometallic imines of rhenium(I) as potential ligands of GSK-3 beta: synthesis, characterization and biological studies, Dalton Trans., 47 (2018) 1233-1242.

[71] D. Giffard, E. Fischer-Fodor, C. Vlad, P. Achimas-Cadariu, G.S. Smith, Synthesis and antitumour evaluation of mono- and multinuclear [2+1] tricarbonylrhenium(I) complexes, Eur. J. Med. Chem., 157 (2018) 773-781.

[72] M. Muñoz-Osses, D. Siegmund, A. Gómez, F. Godoy, A. Fierro, L. Llanos, D. Aravena, N. Metzler-Nolte, Influence of the substituent on the phosphine ligand in novel rhenium(i) aldehydes. Synthesis, computational studies and first insights into the antiproliferative activity, Dalton Trans., 47 (2018) 13861-13869.

[73] C.A. Kumar, R. Nagarajaprakash, W. Victoria, V. Veena, N. Sakthivel, B. Manimaran, Synthesis, characterisation and cytotoxicity studies of Manganese(I) and Rhenium(I) based metallacrown ethers, Inorg. Chem. Commun., 64 (2016) 39-44.
[74] A. François, C. Auzanneau, V. Le Morvan, C. Galaup, H.S. Godfrey, L. Marty, A. Boulay, M. Artigau, B. Mestre-Voegtlé, N. Leygue, C. Picard, Y. Coulais, J. Robert, E. Benoist, A functionalized heterobimetallic 99mTc/Re complex as a potential dual-modality imaging probe: synthesis, photophysical properties, cytotoxicity and cellular imaging investigations, Dalton Trans., 43 (2014) 439-450.
[75] R. Huang, G. Langille, R.K. Gill, C.M.J. Li, Y. Mikata, M.Q. Wong, D.T. Yapp, T. Storr, Synthesis, characterization, and biological studies of emissive rhenium–glutamine conjugates, J. Biol. Inorg. Chem., 18 (2013) 831-844.
[76] A. Monks, D. Scudiero, P. Skehan, R. Shoemaker, K. Paull, D. Vistica, C. Hose, J. Langley, P. Cronise, A. Vaigro-Wolff, M. Gray-Goodrich, H. Campbell, J. Mayo, M. Boyd, Feasibility of a High-Flux Anticancer Drug Screen Using a Diverse Panel of Cultured Human Tumor Cell Lines, J. Natl Cancer I., 83 (1991) 757-766.
[77] R. Fior, V. Póvoa, R.V. Mendes, T. Carvalho, A. Gomes, N. Figueiredo, M.G. Ferreira, Single-cell functional and chemosensitive profiling of combinatorial colorectal therapy in zebrafish xenografts, Proc. Natl. Acad. Sci. USA, 114 (2017) E8234-E8243.
[78] K. Kai, O. Nagano, E. Sugihara, Y. Arima, O. Sampetrean, T. Ishimoto, M. Nakanishi, N.T. Ueno, H. Iwase, H. Saya, Maintenance of HCT116 colon cancer cell line conforms to a stochastic model but not a cancer stem cell model, Cancer Sci., 100 (2009) 2275-2282.
[79] P.M. De Angelis, K.L. Kravik, S.H. Tunheim, T. Haug, W.H. Reichelt, Comparison of gene expression in HCT116 treatment derivatives generated by two different 5-fluorouracil exposure protocols, Mol. Cancer, 3 (2004) 11.
[80] C. Chakraborty, C.H. Hsu, Z.H. Wen, C.S. Lin, G. Agoramoorthy, Zebrafish: A Complete Animal Model for *In vivo* Drug Discovery and Development, Curr. Drug Metab., 10 (2009) 116-124.
[81] C.A. MacRae, R.T. Peterson, Zebrafish as tools for drug discovery, Nat. Rev. Drug Discov., 14 (2015) 721.
[82] I. Ott, X. Qian, Y. Xu, D.H. Vlecken, I.J. Marques, D. Kubutat, J. Will, W.S. Sheldrick, P. Jesse, A. Prokop, C.P. Bagowski, A gold(I) phosphine complex containing a naphthalimide ligand functions as a TrxR inhibiting antiproliferative agent and angiogenesis inhibitor, J. Med. Chem., 52 (2009) 763-770.
[83] A. Pavic, B.D. Glisic, S. Vojnovic, B. Warzajtis, N.D. Savic, M. Antic, S. Radenkovic, G.V. Janjic, J. Nikodinovic-Runic, U. Rychlewska, M.I. Djuran, Mononuclear gold(III) complexes with phenanthroline ligands as efficient inhibitors of angiogenesis: A comparative study with auranofin and sunitinib, J. Inorg. Biochem., 174 (2017) 156-168.
[84] L. Senerovic, M.D. Zivkovic, A. Veselinovic, A. Pavic, M.I. Djuran, S. Rajkovic, J. Nikodinovic-Runic, Synthesis and evaluation of series of diazine-bridged dinuclear platinum(II) complexes through *in vitro* toxicity and molecular modeling: correlation between structure and activity of Pt(II) complexes, J. Med. Chem., 58 (2015) 1442-1451.
[85] F.X. Wang, M.H. Chen, Y.N. Lin, H. Zhang, C.P. Tan, L.N. Ji, Z.W. Mao, Dual Functions of Cyclometalated Iridium(III) Complexes: Anti-Metastasis and Lysosome-Damaged Photodynamic Therapy, ACS Appl. Mater Interfaces, 9 (2017) 42471-42481.
[86] D.S. Jović, M.N. Seke, A.N. Djordjevic, J.Ž. Mrđanović, L.D. Aleksić, G.M. Bogdanović, A.B. Pavić, J. Plavec, Fullerenol nanoparticles as a new delivery system for doxorubicin, RSC Adv., 6 (2016) 38563-38578.
[87] C. de Koning, M. Beekhuijzen, M. Tobor-Kapłon, S. de Vries-Buitenweg, D. Schoutsen, N. Leeijen, B. van de Waart, H. Emmen, Visualizing Compound Distribution during Zebrafish Embryo Development: The Effects of Lipophilicity and DMSO, Birth Defects Res. B Dev. Reprod. Toxicol., 104 (2015) 253-272.

[88] N.A. Ducharme, L.E. Peterson, E. Benfenati, D. Reif, C.W. McCollum, J. Gustafsson, M. Bondesson, Meta-analysis of toxicity and teratogenicity of 133 chemicals from zebrafish developmental toxicity studies, Reprod. Toxicol., 41 (2013) 98-108.
[89] J.K. Leet, C.D. Lindberg, L.A. Bassett, G.M. Isales, K.L. Yozzo, T.D. Raftery, D.C. Volz, High-Content Screening in Zebrafish Embryos Identifies Butafenacil as a Potent Inducer of Anemia, Plos One, 9 (2014) e104190.
[90] P.A. Clarke, T. Roe, K. Swabey, S.M. Hobbs, C. McAndrew, K. Tomlin, I. Westwood, R. Burke, R. van Montfort, P. Workman, Dissecting mechanisms of resistance to targeted drug combination therapy in human colorectal cancer, Oncogene, 38 (2019) 5076-5090.
[91] H. Shen, R.E. Perez, B. Davaadelger, C.G. Maki, Two 4N cell-cycle arrests contribute to cisplatin-resistance, Plos One, 8 (2013) e59848.
[92] A.A. Untereiner, A. Pavlidou, N. Druzhyna, A. Papapetropoulos, M.R. Hellmich, C. Szabo, Drug resistance induces the upregulation of H2S-producing enzymes in HCT116 colon cancer cells, Biochem. Pharmacol., 149 (2018) 174-185.
[93] J. Folkman, Angiogenesis in cancer, vascular, rheumatoid and other disease, Nature Med., 1 (1995) 27-30.
[94] K.A. Rmali, M.C.A. Puntis, W.G. Jiang, Tumour-associated angiogenesis in human colorectal cancer, Colorectal Dis., 9 (2007) 3-14.
[95] N. Ferrara, R.S. Kerbel, Angiogenesis as a therapeutic target, Nature, 438 (2005) 967-974.
[96] J. Yellol, S.A. Pérez, A. Buceta, G. Yellol, A. Donaire, P. Szumlas, P.J. Bednarski, G. Makhloufi, C. Janiak, A. Espinosa, J. Ruiz, Novel C,N-Cyclometalated Benzimidazole Ruthenium(II) and Iridium(III) Complexes as Antitumor and Antiangiogenic Agents: A Structure–Activity Relationship Study, J. Med. Chem., 58 (2015) 7310-7327.
[97] A. Zamora, S.A. Pérez, V. Rodríguez, C. Janiak, G.S. Yellol, J. Ruiz, Dual Antitumor and Antiangiogenic Activity of Organoplatinum(II) Complexes, J. Med. Chem., 58 (2015) 1320-1336.
[98] J. Yang, Q. Cao, H. Zhang, L. Hao, D. Zhou, Z. Gan, Z. Li, Y.-X. Tong, L.-N. Ji, Z.-W. Mao, Targeted reversal and phosphorescence lifetime imaging of cancer cell metabolism via a theranostic rhenium(I)-DCA conjugate, Biomaterials, 176 (2018) 94-105.
[99] A. Albini, G. Pennesi, F. Donatelli, R. Cammarota, S. De Flora, D.M. Noonan, Cardiotoxicity of Anticancer Drugs: The Need for Cardio-Oncology and Cardio-Oncological Prevention, J. Natl. Cancer Inst., 102 (2010) 14-25.
[100] S.L. Beedie, C. Mahony, H.M. Walker, C.H. Chau, W.D. Figg, N. Vargesson, Shared mechanism of teratogenicity of anti-angiogenic drugs identified in the chicken embryo model, Sci. Rep., 6 (2016) 30038-30038.
[101] P. Collery, A. Mohsen, A. Kermagoret, S. Corre, G. Bastian, A. Tomas, M. Wei, F. Santoni, N. Guerra, D. Desmaële, J. d'Angelo, Antitumor activity of a rhenium (I)-diselenoether complex in experimental models of human breast cancer, Invest. New Drugs, 33 (2015) 848-860.
[102] R. Fior, V. Póvoa, R.V. Mendes, T. Carvalho, A. Gomes, N. Figueiredo, M.G. Ferreira, Single-cell functional and chemosensitive profiling of combinatorial colorectal therapy in zebrafish xenografts, Proc. Natl. Acad. Sci. USA, 114 (2017) E8234.
[103] R. White, K. Rose, L. Zon, Zebrafish cancer: the state of the art and the path forward, Nat. Rev. Cancer, 13 (2013) 624-636.
[104] C. Tobia, G. Gariano, G. De Sena, M. Presta, Zebrafish embryo as a tool to study tumor/endothelial cell cross-talk, Biochim. Biophys. Acta Mol. Basis Dis., 1832 (2013) 1371-1377.
[105] S.B. J., O.B. L., C. João, N. Magda, F.M. Godinho, F. Rita, B.G.J. L., Cisplatin-triggered Bioorthogonal Decaging of Amide Bonds for Targeted-Drug Activation *in vivo*, ChemRxiv, (2018).

[106] J. Petrovic, J. Glamoclija, T. Ilic-Tomic, M. Sokovic, D. Robajac, O. Nedic, A. Pavic, Lectin from Laetiporus sulphureus effectively inhibits angiogenesis and tumor development in the zebrafish xenograft models of colorectal carcinoma and melanoma, Int. J. Biol. Macromol., 148 (2020) 129-139.
[107] G. Varricchi, P. Ameri, C. Cadeddu, A. Ghigo, R. Madonna, G. Marone, V. Mercurio, I. Monte, G. Novo, P. Parrella, F. Pirozzi, A. Pecoraro, P. Spallarossa, C. Zito, G. Mercuro, P. Pagliaro, C.G. Tocchetti, Antineoplastic Drug-Induced Cardiotoxicity: A Redox Perspective, Front. Physiol., 9 (2018) 167.
[108] M.E. Shaul, Z.G. Fridlender, Tumour-associated neutrophils in patients with cancer, Nat. Rev. Clin. Oncol., 16 (2019) 601-620.
[109] X. Zhang, W. Zhang, X. Yuan, M. Fu, H. Qian, W. Xu, Neutrophils in cancer development and progression: Roles, mechanisms, and implications (Review), International journal of oncology, 49 (2016) 857-867.
[110] J. Todoric, L. Antonucci, M. Karin, Targeting Inflammation in Cancer Prevention and Therapy, Cancer Prev. Res., 9 (2016) 895.
[111] R.G. Balasingham, M.P. Coogan, F.L. Thorp-Greenwood, Complexes in context: Attempting to control the cellular uptake and localisation of rheniumfac-tricarbonyl polypyridyl complexes, Dalton Trans., 40 (2011) 11663-11674.
[112] K. Yin Zhang, K. Ka-Shun Tso, M.-W. Louie, H.-W. Liu, K.K.-W. Lo, A Phosphorescent Rhenium(I) Tricarbonyl Polypyridine Complex Appended with a Fructose Pendant That Exhibits Photocytotoxicity and Enhanced Uptake by Breast Cancer Cells, Organometallics, 32 (2013) 5098-5102.
[113] A.P. King, S.C. Marker, R.V. Swanda, J.J. Woods, S.-B. Qian, J.J. Wilson, A Rhenium Isonitrile Complex Induces Unfolded Protein Response-Mediated Apoptosis in Cancer Cells, Chem. Eur. J., 25 (2019) 9206-9210.
[114] J.L. Wedding, H.H. Harris, C.A. Bader, S.E. Plush, R. Mak, M. Massi, D.A. Brooks, B. Lai, S. Vogt, M.V. Werrett, P.V. Simpson, B.W. Skelton, S. Stagni, Intracellular distribution and stability of a luminescent rhenium(i) tricarbonyl tetrazolato complex using epifluorescence microscopy in conjunction with X-ray fluorescence imaging, Metallomics, 9 (2017) 382-390.
[115] B.L. Murphy, S.C. Marker, V.J. Lambert, J.J. Woods, S.N. MacMillan, J.J. Wilson, Synthesis, characterization, and biological properties of rhenium(I) tricarbonyl complexes bearing nitrogen-donor ligands, J. Organomet. Chem., 907 (2020) 121064.
[116] R.F. Dielschneider, E.S. Henson, S.B. Gibson, Lysosomes as Oxidative Targets for Cancer Therapy, Oxid. Med. Cell Longev., 2017 (2017) 3749157.
[117] K. Qiu, H. Zhu, T.W. Rees, L. Ji, Q. Zhang, H. Chao, Recent advances in lysosome-targeting luminescent transition metal complexes, Coord. Chem. Rev., 398 (2019) 113010.
[118] N. Fehrenbacher, M. Jaattela, Lysosomes as targets for cancer therapy, Cancer Res., 65 (2005) 2993-2995.
[119] C.G. Towers, A. Thorburn, Targeting the Lysosome for Cancer Therapy, Cancer Discov., 7 (2017) 1218-1220.
[120] R. Halaby, Role of lysosomes in cancer therapy, Res. Rep. Biol., 6 (2015) 147-155.
[121] M.P. Sullivan, M. Groessl, S.M. Meier, R.L. Kingston, D.C. Goldstone, C.G. Hartinger, The metalation of hen egg white lysozyme impacts protein stability as shown by ion mobility mass spectrometry, differential scanning calorimetry, and X-ray crystallography, Chem. Commun., 53 (2017) 4246-4249.
[122] A. Casini, G. Mastrobuoni, C. Temperini, C. Gabbiani, S. Francese, G. Moneti, C.T. Supuran, A. Scozzafava, L. Messori, ESI mass spectrometry and X-ray diffraction studies of adducts between anticancer platinum drugs and hen egg white lysozyme, Chem. Commun., (2007) 156-158.
[123] L. Messori, A. Merlino, Cisplatin binding to proteins: A structural perspective, Coord. Chem. Rev., 315 (2016) 67-89.

[124] I.W. McNae, K. Fishburne, A. Habtemariam, T.M. Hunter, M. Melchart, F. Wang, M.D. Walkinshaw, P.J. Sadler, Half-sandwich arene ruthenium(II)-enzyme complex, Chem. Commun., (2004) 1786-1787.
[125] C. Mugge, T. Marzo, L. Massai, J. Hildebrandt, G. Ferraro, P. Rivera-Fuentes, N. Metzler-Nolte, A. Merlino, L. Messori, W. Weigand, Platinum(II) Complexes with O,S Bidentate Ligands: Biophysical Characterization, Antiproliferative Activity, and Crystallographic Evidence of Protein Binding, Inorg. Chem., 54 (2015) 8560-8570.
[126] Y. Gothe, T. Marzo, L. Messori, N. Metzler-Nolte, Iridium(I) Compounds as Prospective Anticancer Agents: Solution Chemistry, Antiproliferative Profiles and Protein Interactions for a Series of Iridium(I) N-Heterocyclic Carbene Complexes, Chem. Eur. J., 22 (2016) 12487-12494.
[127] G. Ferraro, T. Marzo, M.E. Cucciolito, F. Ruffo, L. Messori, A. Merlino, Reaction with Proteins of a Five-Coordinate Platinum(II) Compound, Int. J. Mol. Sci., 20 (2019).
[128] F. Zobi, B. Spingler, Post-protein-binding reactivity and modifications of the fac-[Re(CO)3]+ core, Inorg. Chem., 51 (2012) 1210-1212.
[129] S.L. Binkley, C.J. Ziegler, R.S. Herrick, R.S. Rowlett, Specific derivatization of lysozyme in aqueous solution with Re(CO)3(H2O)3(+), Chem. Commun., 46 (2010) 1203-1205.
[130] S.L. Binkley, T.C. Leeper, R.S. Rowlett, R.S. Herrick, C.J. Ziegler, Re(CO)(3)(H(2)O)(3)(+) binding to lysozyme: structure and reactivity, Metallomics, 3 (2011) 909-916.
[131] G. Santoro, O. Blacque, F. Zobi, Post-protein binding metal-mediated coupling of an acridine orange-based fluorophore, Metallomics, 4 (2012) 253-259.
[132] F. Zobi, B. Spingler, R. Alberto, Guanine and plasmid DNA binding of mono- and trinuclear fac-[Re(CO)3]+ complexes with amino acid ligands, Chembiochem, 6 (2005) 1397-1405.
[133] C.C. Pagoni, V.S. Xylouri, G.C. Kaiafas, M. Lazou, G. Bompola, E. Tsoukas, L.C. Papadopoulou, G. Psomas, D. Papagiannopoulou, Organometallic rhenium tricarbonyl-enrofloxacin and -levofloxacin complexes: synthesis, albumin-binding, DNA-interaction and cell viability studies, J. Biol. Inorg. Chem., 24 (2019) 609-619.
[134] F. Zobi, B. Spingler, T. Fox, R. Alberto, Toward novel DNA binding metal complexes: Structure and basic kinetic data of [M(9MeG)(2)(CH3OH)(CO)(3)](+) (M=Tc-99, Re), Inorg. Chem., 42 (2003) 2818-2820.
[135] F. Zobi, O. Blacque, H.W. Schmalle, B. Spingler, R. Alberto, Head-to-head (HH) and head-to-tail (HT) conformers of cis-bis guanine ligands bound to the [Re(CO)(3)](+) core, Inorg. Chem., 43 (2004) 2087-2096.
[136] F. Zobi, B. Spingler, R. Alberto, Structure, reactivity and solution behaviour of [Re(ser)(7-MeG)(CO)(3)] and [Re(ser)(3-pic)(CO)(3)]: "nucleoside-mimicking" complexes based on the fac-[Re(CO)(3)](+) moiety, Dalton Trans., (2005) 2859-2865.
[137] F. Zobi, O. Blacque, R.K.O. Sigel, R. Alberto, Binding interaction of [Re(H2O)(3)(CO)(3)](+) with the DNA fragment d(CpGpG), Inorg. Chem., 46 (2007) 10458-10460.
[138] R.R. Varma, B.H. Pursuwani, E. Suresh, B.S. Bhatt, M.N. Patel, Single crystal, DNA interaction and cytotoxicity studies of rhenium(I) organometallic compounds, J. Mol. Struct., 1200 (2020) 127068.
[139] G. Balakrishnan, T. Rajendran, K. Senthil Murugan, M. Sathish Kumar, V.K. Sivasubramanian, M. Ganesan, A. Mahesh, T. Thirunalasundari, S. Rajagopal, Interaction of rhenium(I) complex carrying long alkyl chain with Calf Thymus DNA: Cytotoxic and cell imaging studies, Inorg. Chim. Acta, 434 (2015) 51-59.
[140] S.A. Savage, A.P. Smith, C.L. Fraser, Efficient synthesis of 4-, 5-, and 6-methyl-2,2 '-bipyridine by a Negishi cross-coupling strategy followed by high-yield conversion to bromo- and chloromethyl-2,2 '-bipyridines, J. Org. Chem., 63 (1998) 10048-10051.
[141] R. Alberto, A. Egli, U. Abram, K. Hegetschweiler, V. Gramlich, P.A. Schubiger, Synthesis and Reactivity of [Net4]2[Rebr3(Co)3] - Formation and Structural Characterization of the Clusters

[Net4][Re3(Mu-3-Oh)(Mu-Oh)3(Co)9] and [Net4][Re2(Mu-Oh)3(Co)6] by Alkaline Titration, J. Chem. Soc. Dalton Trans., (1994) 2815-2820.
[142] G.M. Sheldrick, SHELXT - Integrated space-group and crystal-structure determination, Acta Cryst. A, 71 (2015) 3-8.
[143] G.M. Sheldrick, Crystal structure refinement with SHELXL, Acta Cryst. C, 71 (2015) 3-8.
[144] I.K. Voets, W.A. Cruz, C. Moitzi, P. Lindner, E.P. Areas, P. Schurtenberger, DMSO-induced denaturation of hen egg white lysozyme, J. Phys. Chem. B, 114 (2010) 11875-11883.
[145] Y.O. Kamatari, K. Akasaka, T. Konno, M. Kataoka, The methanol-induced transition and the expanded helical conformation in hen lysozyme, Protein Sci., 7 (1998) 681-688.
[146] M.B. Hansen, S.E. Nielsen, K. Berg, Re-examination and further development of a precise and rapid dye method for measuring cell growth/cell kill, J. Immunol. Methods, 119 (1989) 203-210.
[147] S.Ž. Đurić, M. Mojicevic, S. Vojnovic, H. Wadepohl, T.P. Andrejević, N.L. Stevanović, J. Nikodinovic-Runic, M.I. Djuran, B.Đ. Glišić, Silver(I) complexes with 1,10-phenanthroline-based ligands: The influence of epoxide function on the complex structure and biological activity, Inorg. Chim. Acta, 502 (2020) 119357.
[148] OECD, Test No. 236: Fish Embryo Acute Toxicity (FET) Test, OECD Guidelines for the Testing of Chemicals, Section 2, , OECD, (2013).
[149] S.A. Renshaw, C.A. Loynes, D.M.I. Trushell, S. Elworthy, P.W. Ingham, M.K.B. Whyte, A transgenic zebrafish model of neutrophilic inflammation, Blood, 108 (2006) 3976-3978.
[150] G.M. Her, C.-C. Chiang, W.-Y. Chen, J.-L. Wu, *In vivo* studies of liver-type fatty acid binding protein (L-FABP) gene expression in liver of transgenic zebrafish (Danio rerio), FEBS Lett., 538 (2003) 125-133.
[151] Y. Zhang, L. Han, Q. He, W. Chen, C. Sun, X. Wang, X. Chen, R. Wang, C.-D. Hsiao, K. Liu, A rapid assessment for predicting drug-induced hepatotoxicity using zebrafish, J. Pharmacol. Toxicol. Met., 84 (2017) 102-110.
[152] J.-H. He, S.-Y. Guo, F. Zhu, J.-J. Zhu, Y.-X. Chen, C.-J. Huang, J.-M. Gao, Q.-X. Dong, Y.-X. Xuan, C.-Q. Li, A zebrafish phenotypic assay for assessing drug-induced hepatotoxicity, J. Pharmacol. Toxicol. Met., 67 (2013) 25-32.
[153] C. Zhao, X. Wang, Y. Zhao, Z. Li, S. Lin, Y. Wei, H. Yang, A novel xenograft model in zebrafish for high-resolution investigating dynamics of neovascularization in tumors, Plos One, 6 (2011) e21768-e21768.

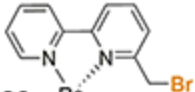

1

4,

LARGE THERAPEUTIC INDEX
TRIPLE ACTIVITY *IN VIVO*